



# 1 **Impacts of irrigation on ozone and fine particulate matter (PM<sub>2.5</sub>) air** 2 **quality: Implications for emission control strategies for intensively** 3 **irrigated regions in China**

4 Tiangang Yuan<sup>1</sup>, Amos P. K. Tai<sup>1,2</sup>, Tzung-May Fu<sup>3</sup>, Aoxing Zhang<sup>3</sup>, David H. Y. Yung<sup>1</sup>, Jin Wu<sup>4</sup>, Sien  
5 Li<sup>5</sup>

6 <sup>1</sup>Earth and Environmental Sciences Programme and Graduate Division of Earth and Atmospheric Sciences, Faculty of Science,  
7 The Chinese University of Hong Kong, Sha Tin, Hong Kong SAR, China

8 <sup>2</sup>State Key Laboratory of Agrobiotechnology and Institute of Environment, Energy and Sustainability, The Chinese University  
9 of Hong Kong, Sha Tin, Hong Kong SAR, China

10 <sup>3</sup>Guangdong Provincial Observation and Research Station for Coastal Atmosphere and Climate of the Greater Bay Area,  
11 School of Environmental Science and Engineering, Southern University of Science and Technology, Shenzhen, Guangdong,  
12 518055, China

13 <sup>4</sup>School of Biological Sciences and Institute for Climate and Carbon Neutrality, The University of Hong Kong, Pok Fu Lam,  
14 Hong Kong SAR, China

15 <sup>5</sup>Center for Agricultural Water Research in China, China Agricultural University, Beijing, 100083, China

16 *Correspondence to:* Amos P. K. Tai (amostai@cuhk.edu.hk)

17 **Abstract.** Intensive irrigation is known to alleviate crop water stress and alter regional climate, which can in turn influence air  
18 quality, with ramifications for human health and food security. However, the interplay between irrigation, climate and air  
19 pollution in especially the simultaneously intensively irrigated and heavily polluted regions in China has rarely been studied.  
20 Here we incorporated a dynamic irrigation scheme into a regional climate-air quality coupled model to examine the potential  
21 impacts of irrigation on ozone (O<sub>3</sub>) and fine particulate matter (PM<sub>2.5</sub>) in China. Results show that irrigation increases the  
22 concentrations of primary air pollutants, but reduces O<sub>3</sub> concentration by 3–4 ppb. PM<sub>2.5</sub>, nitrate and ammonium rise by 28 %,   
23 70 % and 40 %, respectively, upon introducing irrigation, with secondary formation contributing to 5–10 %, ~60 %, and 10–  
24 30 %, respectively. High humidity and low temperature are the top two factors promoting the formation of ammonium nitrate  
25 aerosols. To mitigate these adverse effects on PM<sub>2.5</sub> air quality, we found that a 20 % combined reduction in NH<sub>3</sub> and NO<sub>x</sub>  
26 emissions is more effective compared with individual emission reductions, while the enhancement in O<sub>3</sub> due to the NO<sub>x</sub>  
27 reduction can be completely offset by irrigation itself. Our study highlights the potential benefits of irrigation regarding O<sub>3</sub>



28 pollution but possible problems regarding PM<sub>2.5</sub> pollution under currently prevalent irrigation modes and anthropogenic  
29 emission scenarios, emphasizing the need for an integrated approach to balance water conservation, air pollution, climate  
30 change mitigation and food security in the face of development needs.

## 31 **1 Introduction**

32 Air pollution has become a global environmental concern because of its detrimental effects on human health (e.g.,  
33 Lelieveld et al., 2015), agricultural production (e.g., Tai et al., 2014), ecosystem health (Zhou et al., 2018; Zhu et al., 2022)  
34 and climate (IPCC, 2021), especially in developing countries undergoing rapid urbanization and industrialization such as India  
35 and China. Among the various pollutants, fine particulate matter with diameter < 2.5 μm (PM<sub>2.5</sub>) and surface ozone (O<sub>3</sub>) are  
36 the two primary air pollutants of the most concern in China (Lim et al., 2020; Deng et al., 2022). The annual PM<sub>2.5</sub> concentration  
37 in the North China Plain (NCP) increased steadily to 106 μg m<sup>-3</sup> during 1970–2013, which was three times the annual standard  
38 (35 μg m<sup>-3</sup>) of Chinese Ambient Air Quality Standards Grade II (An et al., 2019). Although it has declined by roughly 40 %  
39 following the implementation of the Air Pollution Prevention and Control Action Plan since 2013 (An et al., 2019; Wang et al.,  
40 2020), more than 65 % of the Chinese people were still exposed to high PM<sub>2.5</sub> in 2018 (Zhao et al., 2021). Meanwhile, the  
41 warm-season (May–September) O<sub>3</sub> showed upward trends of 0.16 and 0.42 ppb yr<sup>-1</sup> during 1981–2019 in NCP and Sichuan  
42 Basin (SCB), respectively (Mao et al., 2024). In recent years, the summertime maximum daily 8-h average O<sub>3</sub> concentration  
43 (MDA8) in China climbed continuously during 2013–2019 (Wang et al., 2022a; Lu et al., 2018). The rising trend is particularly  
44 evident in NCP (3.3 ppb yr<sup>-1</sup>, Li et al., 2020), which was mainly caused by the weakened titration by nitrogen oxides (NO<sub>x</sub> ≡  
45 NO + NO<sub>2</sub>) and aerosol uptake of hydroperoxyl radicals under the context of emission reduction (Li et al., 2019; Wang et al.,  
46 2022b).

47 PM<sub>2.5</sub> consists of primary aerosols such as mineral dust and black carbon (BC), as well as secondary aerosols from gaseous  
48 precursors including secondary organic aerosols (SOA) and secondary inorganic aerosols (SIA, e.g., nitrate, sulfate and  
49 ammonium), while surface O<sub>3</sub> is mainly produced by its precursors including NO<sub>x</sub>, volatile organic compounds (VOCs) and  
50 carbon monoxide (CO) through photochemical oxidation in the presence of sunlight. There is complicated non-linear response  
51 of O<sub>3</sub> and PM<sub>2.5</sub> to emission reduction and meteorological conditions. During the COVID-19 when the large reduction in NO<sub>x</sub>



52 emission enhanced atmospheric oxidative capacity, the level of secondary  $PM_{2.5}$  and surface  $O_3$  rose in megacity clusters of  
53 China including NCP and SCB, although the lockdown effectively reduced primary  $PM_{2.5}$  concentration (Huang et al., 2021;  
54 Shi et al., 2021).

55 Le et al. (2020) and Wang et al. (2022c) argued that the contribution of meteorological factors to the enhancement of  $O_3$   
56 and  $PM_{2.5}$  may outweigh the impact of  $NO_x$  reduction in eastern China during the lockdown. Furthermore, considerable studies  
57 indicate that meteorological conditions make up approximately 10–70 % of  $PM_{2.5}$  variability and 49–84 % of summertime  $O_3$   
58 increase in China, outweighing the contribution of anthropogenic emissions (Dang et al., 2021; Yin et al., 2021; Leung et al.,  
59 2018). Meteorological factors influence  $O_3$  and  $PM_{2.5}$  through various pathways. For instance, low planetary boundary layer  
60 height (PBLH) and wind speed can trap all pollutants near the surface, and high relative humidity (RH) promotes SIA formation  
61 through heterogeneous reactions and aerosol hygroscopic growth, although heavy precipitation causes wet scavenging that  
62 removes aerosols and other gaseous pollutants (Chen et al., 2020; Zhang et al., 2015; Tie et al., 2017). Moreover, high  
63 temperature can enhance biogenic VOC emissions, accelerate  $SO_2$  oxidation and other photochemical reactions, thereby  
64 increasing sulfate,  $O_3$  and SOA. However, it usually has the opposite effect on nitrate, shifting it from the aerosol to gas phase  
65 (Tai et al., 2010; Shi et al., 2020). High temperatures are also usually associated with subtropical highs, which can generate  
66 stagnation events that tend to trap air pollutants and worsen air quality (Tai et al., 2010, 2012). Therefore, meteorological  
67 conditions are crucial in determining regional air quality through both physical and chemical processes.

68 Large-scale irrigation in agriculture has been shown to modify boundary meteorology substantially via enhancing  
69 evapotranspiration directly and provoking land-atmospheric feedback indirectly (McDermid et al., 2023). Specifically,  
70 evapotranspiration induced by irrigation can reduce surface air temperature, increase RH and cloud cover, and contribute to  
71 cloud formation. These effects, in turn, can stabilize and lower atmospheric boundary layer (e.g., Cook et al., 2015; Qian et al.,  
72 2020). Yuan et al. (2023) demonstrated that through these processes, flood and sprinkler irrigation in NCP can enhance  
73 convective precipitation by raising convective available potential energy (CAPE) and precipitable water, whereas drip  
74 irrigation may cause a distinct hydrometeorological feedback and further suppress summertime precipitation slightly. These  
75 meteorological changes induced by irrigation may then affect  $O_3$  and  $PM_{2.5}$  pollution, but only very few studies thus far have  
76 examined the relationships between irrigation, climate and air pollution. Jacobson (1999) first found that initializing the



77 coupled meteorology-chemistry model with high soil moisture thins the PBLH and increases surface air pollutants including  
78 O<sub>3</sub> in Los Angeles. By adding irrigation water into the soil directly to mimic irrigation, Jacobson (2008) showed that the PM<sub>2.5</sub>  
79 and O<sub>3</sub> could increase by approximately 2 % and 0.1 %, respectively, in California. Li et al. (2016) incorporated a dynamic  
80 irrigation method into the Weather Research and Forecasting with Chemistry (WRF-Chem) model and found that irrigation  
81 enhanced the concentrations of surface primary pollutants such as carbon monoxide (CO) and VOCs, but reduced O<sub>3</sub> slightly  
82 over irrigated areas in the Central Valley of California. The enhanced divergence over irrigated areas further transported  
83 pollutants from irrigated regions to nearby non-irrigated areas, leading to relatively higher O<sub>3</sub> concentrations in the surrounding  
84 areas. In addition, irrigation may affect natural emissions including soil NO<sub>x</sub> and soil ammonia (NH<sub>3</sub>) by altering soil moisture  
85 and temperature, which are essential precursors of PM<sub>2.5</sub> and O<sub>3</sub> (Shen et al., 2023; Song et al., 2021). Thus, large-scale  
86 irrigation may exert important but under-researched roles in modulating regional air quality.

87 China currently possesses the largest irrigated cropland area in the world, whereby the irrigated area expanded dramatically  
88 from ~16 to ~68 Mha during 1949–2017, consuming over 70 % fresh water (Han et al., 2020a). The rapid irrigation expansion  
89 has caused water scarcity and depletion of groundwater storage, threatening food security and natural ecosystems (Currell et  
90 al., 2012). NCP and SCB are the two regions with intensively irrigated areas, high food production as well as severe air  
91 pollution in China. Considerable research efforts have been devoted to the effects of irrigation on crop yields based on crop,  
92 hydrological or land surface models, and on hydrometeorology based on global or regional climate models (McDermid et al.,  
93 2023), while relatively little attention has been paid to the nonlinear interactions between irrigation, meteorology and air  
94 pollution. Moreover, a deeper understanding of such complicated interactions is essential to the co-formulation of effective air  
95 quality and agricultural management strategies, not only because irrigation can affect air quality, but also because high  
96 agricultural production contributes significant amounts of NH<sub>3</sub> to the atmosphere, which is an important precursor of PM<sub>2.5</sub> in  
97 these two regions. To address these questions, we incorporated a dynamic irrigation scheme into a coupled climate-air quality  
98 model, the Weather Research and Forecasting (WRF) meteorological model (v3.9.1.1) coupled with the GEOS-Chem chemical  
99 transport model (v12.7.2) (WRF-GC v2.0, Feng et al., 2021). This study represents the first comprehensive assessment of the  
100 possible impacts of irrigation on O<sub>3</sub> and PM<sub>2.5</sub> in China, and proposes effective emission control strategies to counteract the  
101 corresponding adverse effects, which would be helpful for policymakers and farmers to evaluate the co-benefits and trade-offs



102 between agricultural and air quality management practices, especially with the rising application of water-saving irrigation  
103 systems in these intensively irrigation areas.

## 104 **2 Data and Methodology**

### 105 **2.1 General model configuration**

106 The WRF-GC model is a newly developed regional climate-atmospheric chemistry model (Lin et al., 2020; Feng et al.,  
107 2021), in which the GEOS-Chem chemical transport model is coupled to the WRF model, a mesoscale weather model for  
108 atmospheric research and weather forecast (Skamarock et al., 2008). Currently, the WRF-GC v2.0 simulates online interactions  
109 and feedbacks between meteorology and chemistry, and considers a vast array of physical and chemical processes including  
110 emission, transport, deposition and chemistry, with multiple parameterization options. It enables users to examine land-  
111 atmosphere physical and chemical interactions at high spatial resolutions. The standard chemical mechanism includes detailed  
112  $O_x$ - $NO_x$ -VOC-ozone-halogen-aerosol chemistry in the troposphere as inherited from GEOS-Chem model. Some aerosol  
113 species such as SIA, SOA, BC and primary organic carbon (POC) are treated as bulk masses by assuming a lognormal size  
114 distribution, while dust and sea salt aerosols are divided into four and two size bins, respectively. The thermodynamical  
115 equilibrium of SIA is simulated by ISORROPIA II module (Pye et al., 2009). The “simple SOA” scheme without detailed  
116 chemical processes was used to simulate SOA yields (Hodzic and Jimenez, 2011; Kim et al., 2015), whereby SOA formation  
117 is directly related to emissions at fixed yields and shows no dependence on other factors such as temperature and  $NO_x$   
118 concentration. For detailed description and evaluation of WRF-GC one can be referred to Lin et al. (2020) and Feng et al.  
119 (2021), who proved that WRF-GC demonstrates satisfactory performance against observations regarding the magnitudes and  
120 spatial patterns of air pollutants, cloud properties and meteorological fields over China.

121 Figure 1a shows our model domain, which covers the intensively irrigated areas including NCP and SCB at a horizontal  
122 resolution of 27 km. Model vertical levels are divided into 50 layers from the surface to 10 hPa. Anthropogenic emissions  
123 including BC, POC, CO,  $NH_3$  and VOCs are derived from the MIX emission inventory for Asia (Li et al., 2017a), overwritten  
124 by monthly Multi-resolution Emission Inventory for China (MEIC) version 1.3 of 2017 at a resolution of  $0.25^\circ$  over China



125 (<http://meicmodel.org.cn>, last access: 1 May 2024; Li et al., 2017b; Zheng et al., 2018). MEIC accounts for emissions from  
126 five sectors: power plant, residential activities, transportation, industry and agriculture; data are available from 2008 to 2017.  
127 Monthly biomass burning emissions are taken from the Global Emissions Database version 4 (GFED4, Randerson et al., 2018).  
128 Biomass emissions, soil NO<sub>x</sub> and dust emissions are calculated online by the Model of Emissions of Gases and Aerosols from  
129 Nature version 2.1 (MEGAN2.1, Guenther et al., 2012), Berkeley–Dalhousie Soil NO<sub>x</sub> Parameterization (BDSNP) (Hudman  
130 et al., 2012) and dust entrainment and deposition (DEAD, Zender et al., 2003), respectively, in the Harmonized Emissions  
131 Component (HEMCO) module. The initial and boundary meteorological conditions are provided by ERA5 reanalysis data  
132 with a spatial resolution of 0.25° and 6-h temporal interval (<https://cds.climate.copernicus.eu/cdsapp#!/home>, last access: 1  
133 May 2024). Initial and boundary conditions of chemical species were obtained from the GEOS-Chem Classic global model  
134 outputs, which uses the same chemical mechanisms and emissions as WRF-GC but at 2×2.5° resolution and with a 1-year  
135 spin-up time. The physical schemes used here are listed in **Table 1**, which have been tested and verified systematically by Feng  
136 et al. (2021).

137

138 **Table 1. Model configuration**

Physical process	Schemes
Microphysics	Morrison two-moment scheme (Morrison et al., 2009)
Cumulus parameterization	New Tiedtke (Tiedtke, 1989; Zhang et al., 2011)
Shortwave radiation	RRTMG (Iacono et al., 2008)
Longwave radiation	RRTMG (Iacono et al., 2008)
Land surface	Noah-MP (Niu et al., 2011)
Planetary boundary layer	Mellor-Yamada Nakanishi and Niino Level 2.5 (Nakanishi and Niino, 2006)

139



## 140 2.2 Irrigation scheme

141 Previous work has documented the parameterization of irrigation in numerical models, which can be characterized by  
142 three major methods. The first approach involves maintaining the soil moisture at different percentages of soil field capacity  
143 or saturation point during the growing season (e.g., Lobell et al., 2008). This method keeps a high soil moisture, which can  
144 cause a cool bias and is deemed unrealistic (Kanamaru and Kanamitsu, 2008). The second one is to derive a time-invariant  
145 irrigation rate based on census irrigation water use (IWU) data (e.g., Sacks et al., 2009; Liu et al., 2021a), but it ignores the  
146 feedbacks from weather and climate on irrigation itself. The last one is a dynamic irrigation method that mimics real irrigation  
147 processes regarding irrigation water amount and ways of water application (e.g., Leng et al., 2017; Yuan et al., 2023). It has  
148 been suggested that the dynamic irrigation method can improve simulated surface energy fluxes, temperature and humidity  
149 greatly, particularly at fine resolutions (Sorooshian et al., 2014; Qian et al., 2020). Therefore, we followed He et al. (2023) and  
150 implemented the dynamic irrigation schemes into the Noah land surface model with multiparameterization (Noah-MP, Niu et  
151 al., 2011) embedded within WRF-GC.

152 Our previous work has investigated the climate effects of different irrigation methods, i.e., flood, sprinkler and drip  
153 irrigation over NCP based on the dynamic irrigation schemes using WRF alone, and found that flood and sprinkler irrigation  
154 have comparable effects on air temperature and precipitation, except that flood irrigation is associated with a larger irrigation  
155 amount and surface runoff (Yuan et al., 2023). Hence, following previous studies, we used sprinkler irrigation method to  
156 represent present-day irrigation in China to avoid the excess water use in the model (e.g., Liu et al., 2021b; Yang et al., 2015).  
157 The irrigation water amount,  $I$  (mm), is the water available between field capacity and current soil moisture, weighted by the  
158 irrigated area fraction (IF) and green vegetation fraction (GVF), when the relative soil moisture is below the management  
159 allowable deficit (MAD), following:

$$160 \quad I = (SM_{fc} - SM) \times DZS \times 1000 \times IF \times GVF \quad \text{if} \quad \frac{SM - SM_{wt}}{SM_{fc} - SM_{wt}} < MAD, \quad (1)$$

161 where  $SM_{fc}$  and  $SM_{wt}$  are soil moisture at soil field capacity and wilting point, respectively;  $SM$  is current soil moisture;  $DZS$   
162 denotes root zone depth (m).  $MAD$  is set at 60%, which is in line with the setting of Yuan et al. (2023). In sprinkler irrigation,  
163 water is applied over the canopy as precipitation. Under this circumstance, part of the water is intercepted by the canopy and



164 evaporates to atmosphere before reaching the ground. Irrigation rate (IR, mm) at each timestep is limited to the minimum of  
165 infiltration ( $i$ , mm), irrigation amount and the rate of  $5 \text{ mm h}^{-1}$  ( $SI_{\text{rate}}$ ) used in Lawston et al. (2015):

$$166 \quad IR = \min(i, I, SI_{\text{rate}} \times \Delta t), \quad (2)$$

167 where  $\Delta t$  is timestep. The evaporative loss ( $E$ , %) from spraying during application is parameterized as the function of wind  
168 speed ( $u$ ,  $\text{m s}^{-1}$ ), saturation vapor pressure ( $e_s$ , hPa), actual vapor pressure ( $e$ , hPa) and surface air temperature ( $T_a$ , °C),  
169 following Bavi et al. (2009):

$$170 \quad E = 4.375 \exp(0.106u) (e_s - e)^{-0.092} T_a^{-0.102}, \quad T_a > 0 \quad (3)$$

$$171 \quad E = 4.337 \exp(0.077u) (e_s - e)^{-0.098}, \quad T_a < 0 \quad (4)$$

172 The model checks if irrigation can be triggered at each timestep during the growing season. Five conditions need to be  
173 met before scheduling irrigation: (1) IF > 10%; (2) precipitation <  $1 \text{ mm h}^{-1}$ ; (3) leaf area index (LAI) > 0.3; (4)  $\frac{SM - SM_{\text{wt}}}{SM_{\text{fc}} - SM_{\text{wt}}} <$   
174 MAD; and (5) land type is cropland.

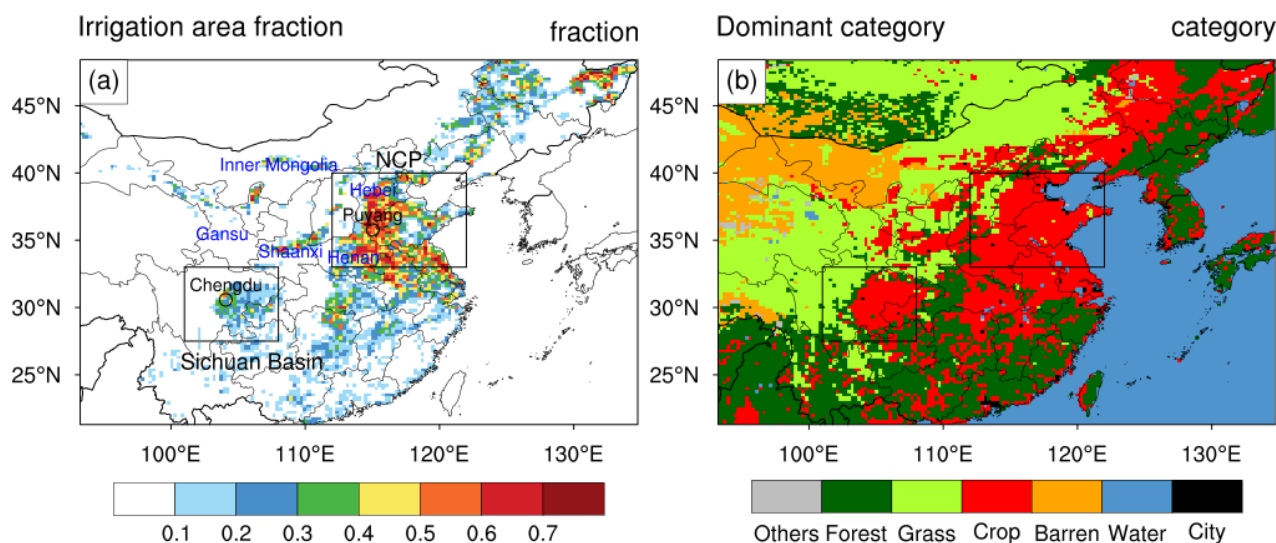
175 To represent irrigation more realistically, we used the actual 500-m irrigation map of 2017 and National Land Cover  
176 Dataset of China (NLCD) in 2015 for China (Fig. 1), which were available from Zhang et al. (2022) and the National Tibetan  
177 Plateau Data Center (<http://data.tpdc.ac.cn>, last access: 1 May 2024), respectively. The irrigated cropland map was generated  
178 by integrating statistics, satellite remote sensing and existing irrigation maps, and has an overall accuracy of 73–82 % against  
179 5648 samples collected from ground-truth images, surpassing the accuracy of other existing irrigation data. The biggest  
180 advantage is that it represents the area that is actually irrigated in a year. The NLCD land cover dataset with 1 km resolution  
181 was produced based on Landsat Thematic Mapper (TM) or Enhanced TM Plus (ETM+) digital images via a human-computer  
182 interaction approach and has more than 90 % overall accuracy based on field surveys (Liu et al., 2014). The land cover was  
183 then converted to 24-category US Geological Survey (USGS) land cover types as model input. Since the model default LAI  
184 and GVF are outdated, we updated them with 8-day composite LAI and GVF from the Global Land Surface Satellite (GLASS)  
185 product at  $0.05^\circ$  (<http://www.glass.umd.edu/Download.html>, last access: 1 May 2024; Liang et al., 2021), which were  
186 processed based on the Moderate-resolution Imaging Spectrometer (MODIS) satellite products. It has been shown that these  
187 products have the best accuracy and quality than other products such as GEOV1 (the first version of Geoland2 satellite





188 products), by comparing with ground observations of LAI and GVF (Li et al., 2018; Jia et al., 2018). They were linearly  
 189 interpolated from 8-day time intervals into daily products for model input.

190



191

192 **Figure 1. Spatial distribution of (a) irrigated area fraction and (b) land use and land cover as WRF-GC model input.**  
 193 **Intensively irrigated areas such as the North China Plain (NCP) and Sichuan Basin (SCB) are squared. Two cities in**  
 194 **the irrigated areas, Puyang and Chengdu, have been selected for further analysis. Some relevant provinces including**  
 195 **Hebei, Henan, Gansu, Shaanxi and Inner Mongolia, are marked in blue fonts.**

196

### 197 2.3 Model experiments

198 Before examining the irrigation effects, we conducted a standard experiment with grid nudging (CTL) to show the ability  
 199 of default WRF-GC model to simulate atmospheric physical and chemical variables. Subsequently, two sensitive experiments,  
 200 one with the irrigation scheme described above (IRR) and one without irrigation (NOIRR) were designed and conducted. To  
 201 clearly show the causality of irrigation and air quality, the climate effects of aerosols (i.e., aerosol-cloud interaction and aerosol-  
 202 radiation interaction) and nudging were switched off in the sensitivity experiments. Therefore, the differences between IRR  
 203 and NOIRR directly indicate how irrigation modifies meteorology and thus affects emission, transport, chemistry and



204 deposition of air pollutants, and the experimental design decidedly did not address how changes in stimulated atmospheric  
205 species that are climate forcers (e.g., aerosols) would further modulate climate in the same model experiment.

206 Since we found that irrigation promotes nitrate formation and further worsens  $PM_{2.5}$  pollution through the above  
207 experiments, we then performed four additional sensitivity experiments to identify the suitable mitigation strategies. The four  
208 experiments used the same settings as IRR but with 20 % and 50 % combined reduction for  $NH_3$  and  $NO_x$ , and 50 % individual  
209 emission reduction for  $NH_3$  and  $NO_x$ , respectively, given that previous studies have highlighted the effectiveness of the  
210 emission reductions in  $NH_3$  and  $NO_x$  in reducing  $PM_{2.5}$  pollution (Zhai et al., 2021; Liu et al., 2021c). In addition, considering  
211 the demanding computational resources required for WRF-GC, we had to choose a study year with relatively normal climate  
212 conditions to reduce the possible influences of interannual climate variability. Due to the limited availability of measurements  
213 of air pollutants in China, which are mostly accessible from 2014 onwards, and the occurrence of the COVID-19 pandemic  
214 during 2019–2022, we ultimately selected the summer of 2017, which had an absolute Standardized Precipitation  
215 Evapotranspiration Index (SPEI) being below 0.5 in NCP and SCB (see summertime SPEI from 2014 to 2018 in Fig. S1).  
216 Indeed, the simulated effects of irrigation on regional climate are similar to the longer-term simulations in our previous work  
217 (Yuan et al., 2023), reflecting small effects of interannual variability of climate on our model results. All seven simulations  
218 were conducted from 1<sup>st</sup> May to 1<sup>st</sup> September 2017, with the first month as model spin-up. Only the results for the summer of  
219 2017 were analyzed.

## 220 **2.4 Observations**

221 The monthly land surface temperature (LST) with a spatial resolution of  $0.05^\circ$  from MODIS onboard Aqua and Terra  
222 (<https://ladsweb.modaps.eosdis.nasa.gov/>, last access: 1 May 2024) were used for model validation. Daily air temperature ( $T_2$ )  
223 recorded by weather stations were derived from the National Oceanic and Atmospheric Administration (NOAA)-National  
224 Climatic Data Center (NCDC) (<ftp://ftp.ncdc.noaa.gov/pub/data/gsd/>, last access: 1 May 2024). The hourly concentrations of  
225 surface air pollutants including  $O_3$  and  $PM_{2.5}$  monitored in sites during 2017 were collected from the Chinese Ministry of  
226 Ecology and Environment (MEE) (archived in <https://quotsoft.net/air/>, last access: 1 May 2024). Here we chose 1334  
227 monitoring sites with valid values over 90 % falling within model domain in the summer of 2017 to evaluate the model results.



228 The monthly SPEI with 3-month timescale for the period 2014–2018 at a spatial resolution of  $0.5^\circ$  considered in this study  
229 was provided by the SPEIbase (<https://digital.csic.es/handle/10261/332007>, last access: 1 May 2024), which has been widely  
230 used to indicate drought characteristics. It was generated through monthly gridded potential evapotranspiration and  
231 precipitation from Climatic Research Unit of the University of East Anglia (Beguería et al., 2010) and a value ranging from  
232  $-0.5$  to  $0.5$  is characterized as normal climate conditions.

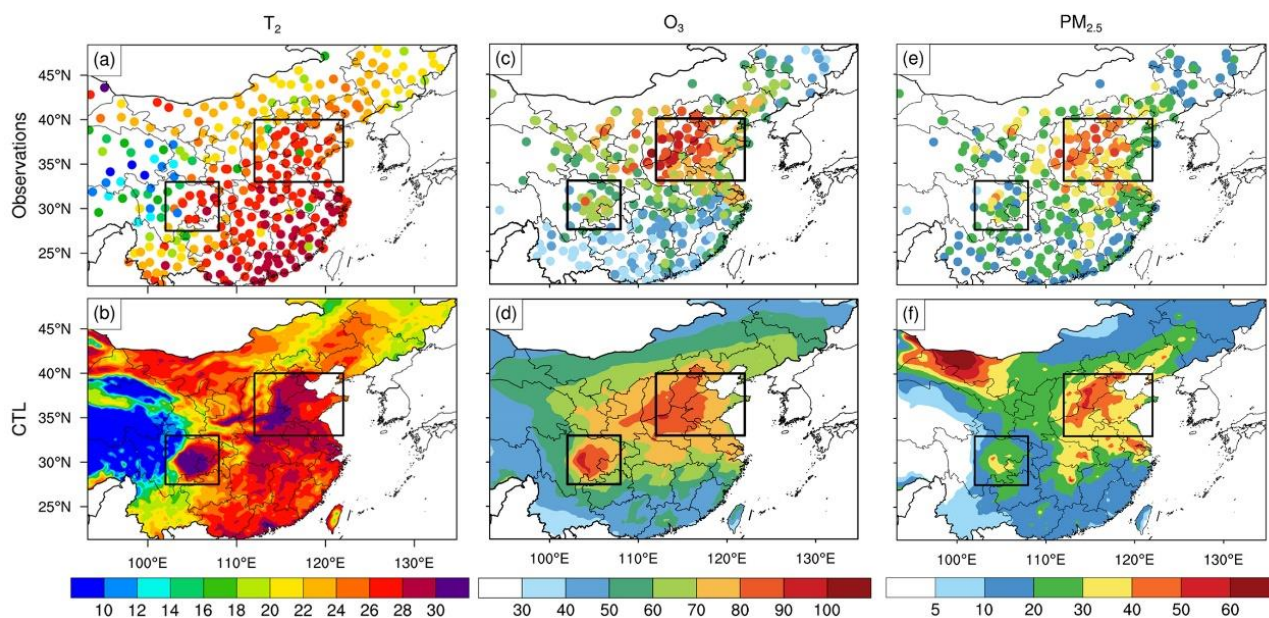
## 233 3 Results

### 234 3.1 Model evaluation

235 **Figure 2** compares the simulated seasonal mean  $T_2$ ,  $PM_{2.5}$  and afternoon  $O_3$  and from CTL with surface observations  
236 during summer. The observed air temperature is around  $28\text{--}30^\circ\text{C}$  in South China and decreases to  $\sim 20^\circ\text{C}$  in the north. The  
237 lowest air temperature is observed in western China because of the high altitude of the Tibetan Plateau. The WRF-GC model  
238 reproduces the spatial pattern and captures the warmer NCP and SCB, with the spatial correlation of 0.85 and Root Mean  
239 Squared Error (RMSE) of  $2.9^\circ\text{C}$ . However, the regional average temperature from the model is  $27.7$  and  $26.3^\circ\text{C}$  in NCP and  
240 SCB, about  $2^\circ\text{C}$  larger than the corresponding observations (Table 2). This warm bias has been reported in many studies and  
241 can be reduced by including irrigation in the model processes (Yang et al., 2015; Qian et al., 2020).

242 We compared the simulated LST from IRR and NOIRR with MODIS LST to quantify the ability of irrigation processes  
243 to reduce model biases (**Figure 3**). The large positive differences of LST between MODIS and NOIRR indicate that the default  
244 model overestimates the LST greatly with the biases more than  $2^\circ\text{C}$  in Northeast China, Central China, Southwest China, and  
245 parts of South China (Fig. 3a). When irrigation is introduced in the model, such warm biases almost disappear in the intensively  
246 irrigated areas including Northeast China, Inner Mongolia, Ningxia, Shaanxi, NCP and SCB (Fig. 3b). The largest  
247 improvements primarily occur in the southern part of NCP and the whole SCB where the biases are reduced by more than  $2^\circ\text{C}$ ,  
248 suggesting that irrigation should be properly represented in numerical models to more accurately simulate meteorological  
249 variables in intensively irrigated regions (Yuan et al., 2023).

250



251

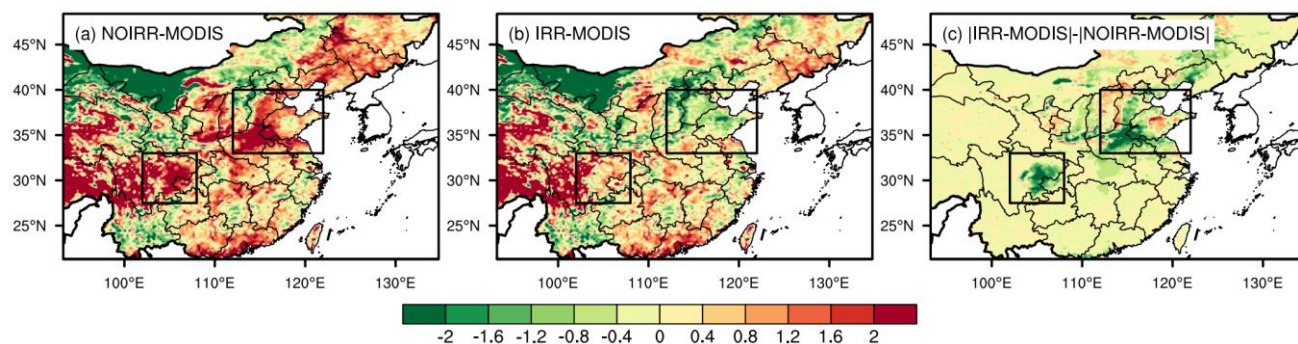
252

253

254

255

**Figure 2. Spatial distribution of (a–b) air temperature at 2m ( $T_2$ , °C), (c–d) surface afternoon (13:00–17:00, Beijing time) ozone ( $O_3$ , ppb) and (e–f) daily mean fine particulate matter ( $PM_{2.5}$ ,  $\mu g\ m^{-3}$ ) derived from surface observations and control (CTL) experiment during the summer of 2017.**



256

257

258

259

260

261

**Figure 3. Spatial distribution of the differences of land surface temperature (LST, °C) between (a) sensitivity experiment without irrigation (NOIRR) and MODIS, (b) sensitivity experiment with irrigation (IRR) and MODIS, and (c) the differences between (a) and (b) during the summer of 2017, which quantitatively show how much the irrigation scheme can reduce the default warm biases. Negative values denote model improvements, while positive values indicate deterioration.**



262

263 **Table 2. Daily mean surface temperature ( $T_2$ ), fine particulate matter ( $PM_{2.5}$ ) and afternoon ozone ( $O_3$ ) from**  
264 **observations and the control (CTL) experiment over North China Plain (NCP) and Sichuan Basin (SCB) during the**  
265 **summer of 2017.**

		NCP	SCB
$T_2$ (°C)	Observation	25.6	24.3
	CTL	27.7	26.3
Afternoon $O_3$ (ppb)	Observation	78.9	61.8
	CTL	78.0	81.8
$PM_{2.5}$ ( $\mu\text{g m}^{-3}$ )	Observation	41.2	25.4
	CTL	42.6	27.4

266

267 We also calculated the concentrations of afternoon surface  $O_3$  (13:00–17:00, Beijing time) and daily mean surface  $PM_{2.5}$   
268 in NCP and SCB. Observations show that peak  $O_3$  concentration primarily appears in NCP, especially in the Hebei and northern  
269 Henan provinces, where  $O_3$  is 90–100 ppb (Fig. 2c). The  $O_3$  in SCB is lower than that in NCP, ranging from 60 to 70 ppb, with  
270 a few sites exhibiting much higher values. Likewise,  $PM_{2.5}$  pollution is severe in NCP where the maximum concentration of  
271 40–60  $\mu\text{g m}^{-3}$ , but it is relatively weaker in SCB (20–40  $\mu\text{g m}^{-3}$ ) (Fig. 2e). The WRF-GC model successfully captures the  
272 hotspots of  $O_3$  and  $PM_{2.5}$  with spatial correlation of 0.78 and 0.70 and RMSE of 11.9 ppb and 8.5  $\mu\text{g m}^{-3}$  across the whole  
273 domain, respectively (Fig. 2d, f). The simulated  $O_3$  and  $PM_{2.5}$  are 77.8 ppb and 40  $\mu\text{g m}^{-3}$  in NCP, respectively, which closely  
274 aligns with observations (78.9 ppb and 41.2  $\mu\text{g m}^{-3}$ ) (Table 2). Similarly, good performance for WRF-GC-simulated  $PM_{2.5}$  was  
275 also found by Feng et al. (2021) focusing on the January of 2015 in NCP. In SCB, the simulated mean  $PM_{2.5}$  is 27.4  $\mu\text{g m}^{-3}$ ,  
276 slightly larger than observation (25.4  $\mu\text{g m}^{-3}$ ). However, the model overestimates the regional averaged  $O_3$  by approximately  
277 20 ppb, although it is close to the biases (13 ppb) reported by Feng et al. (2021) using WRF-GC for the entire China. It is a

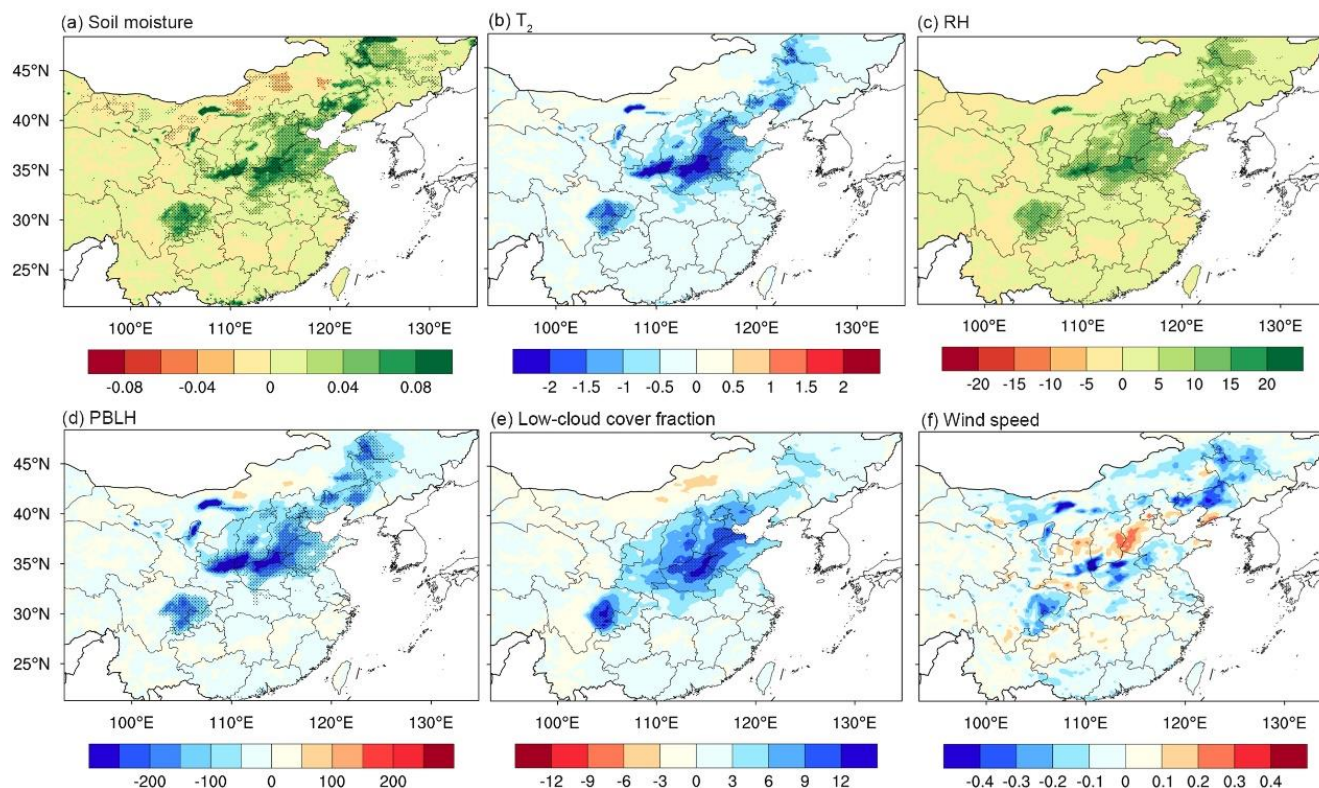


278 common issue for GEOS-Chem to overestimate the summertime surface O<sub>3</sub> in China (Dang et al., 2021; Ye et al., 2022), which  
279 can be attributable to coarse resolution of the model and emission inventories, large stratosphere-troposphere exchange, low  
280 cloud cover and precipitation, and rapid chemical conversion, as summarized by Yang and Zhao (2023) who reviewed the  
281 performance of several popular air quality models. Ye et al. (2022) confirmed that the low cloud optical depth and small O<sub>3</sub>  
282 dry deposition rate in GEOS-Chem are responsible for the overestimation of O<sub>3</sub>, particularly in SCB. Therefore, the  
283 uncertainties inherited from GEOS-Chem may lead to the larger overestimation of O<sub>3</sub> in SCB. Overall, WRF-GC is able to  
284 reproduce the meteorological fields and chemical variables, despite overestimation of O<sub>3</sub> in SCB. These systematic biases are  
285 fully considered in our sensitivity simulations to investigate and interpret the effects of irrigation on atmospheric chemistry.

### 286 3.2 Impacts of irrigation on boundary meteorology

287 **Figure 4** illustrates the differences in meteorological conditions between IRR and NOIRR. Irrigation increases soil  
288 moisture by around 0.04–0.08 m<sup>3</sup> m<sup>-3</sup> over irrigated areas in NCP and SCB. High soil moisture enhances soil evaporation and  
289 crop transpiration, cooling the surface air temperature by 1–2 °C and increasing RH by around 10–20 % in NCP. Such changes  
290 are relatively weaker in SCB because of the lower irrigation intensity. The enhancement of evapotranspiration due to irrigation  
291 increases latent heat flux but reduces sensible heat flux (not shown), leading to a decline of over 250 m and 150 m in PBLH  
292 over NCP and SCB, respectively (Fig. 4d). The low-cloud cover increases by 9–12 % significantly over both NCP and SCB  
293 (Fig. 4e). The reduction of downward solar radiation in response to cloud formation is up to 10 W m<sup>-2</sup> (Fig. S2), in good  
294 consistency with our previous long-term simulation results (Yuan et al., 2023), albeit being statistically insignificant.  
295 Additionally, the stable atmosphere associated with irrigation reduces the surface wind speed, with significant reduction of  
296 0.2–0.4 m s<sup>-1</sup> in part of the irrigated areas (Fig. 4f), implying more unfavorable meteorological conditions for the dissipation  
297 of air pollutants.

298



299

300

301

302

303

304

305

306

307

308

309

310

311

**Figure 4.** Spatial distribution of changes in topsoil moisture ( $\text{m}^3 \text{m}^{-3}$ ), 2 m air temperature ( $T_2$ , °C), 2 m relative humidity (RH, %), planet boundary layer height (PBLH, m), low-cloud fraction (%) and 10-m wind speed ( $\text{m s}^{-1}$ ) in IRR relative to NOIRR during the summer of 2017. The dotted area indicates changes that are statistically significant at 95% confidence level using two-tailed Student's  $t$ -test.

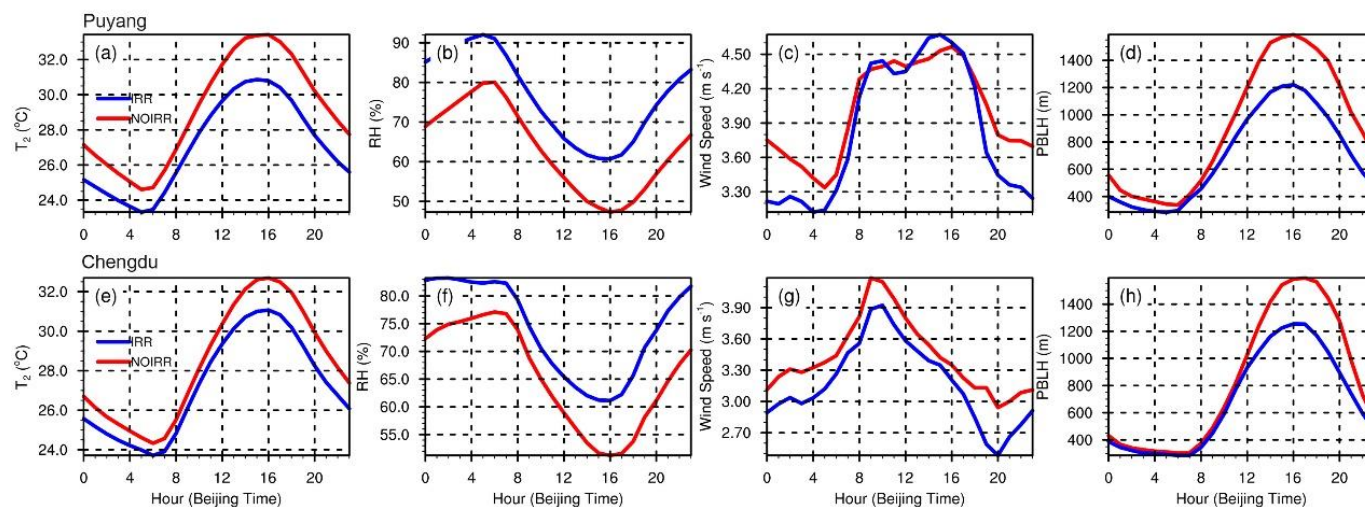
**Figure 5** shows the diurnal cycle of meteorological conditions from IRR and NOIRR in two cities, Puyang and Chengdu, situated in the irrigated regions in NCP and SCB, respectively. In NOIRR,  $T_2$  and PBLH reach a maximum at 15:00–16:00, but RH drops to a minimum in these two cities around the same time. In Puyang, strong wind speeds occur at 15:00–16:00, while in Chengdu, they occur at 9:00–10:00. When irrigation is considered, the reduction in  $T_2$  and increase in RH are obvious throughout the whole day with the remarkable changes reaching up to  $-2.5$  °C and 16 %, respectively, during their peak time in Puyang. Similar changes are also seen in Chengdu but with comparatively smaller values ( $-1.6$  °C and 10 %, respectively). The reductions in wind speed and PBLH mainly occur at midnight and afternoon, respectively, with the changes reaching 0.2–



312 0.5 m s<sup>-1</sup> and 400 m, in these two regions.

313 **Figure 6** displays the vertical profiles of daily average meteorological fields and pollutants in Puyang. Irrigation strongly  
 314 lowers the potential temperature but increases RH below 1.7 km by up to 2 °C and 12 %, respectively, making the slope of  
 315 potential temperature with height steeper and thus stabilizing and moistening the boundary layer greatly (Fig. 6a, b).  
 316 Additionally, the RH in IRR is reduced slightly over the altitude of 1.7 km in comparison to the NOIRR because of the more  
 317 stable atmosphere. Chengdu is influenced by irrigation slightly with the variations of up to -1 °C and 4 % in potential  
 318 temperature and RH (Fig. S3a, b). Consequently, a more stable, moister, cooler and shallower boundary layer is formed over  
 319 all irrigated areas and adjacent non-irrigated areas. Overall, irrigation has substantial effects on daytime temperature and PBLH,  
 320 as well as nocturnal wind speed, whereas the effects on RH are comparable during daytime and nighttime.

321



322

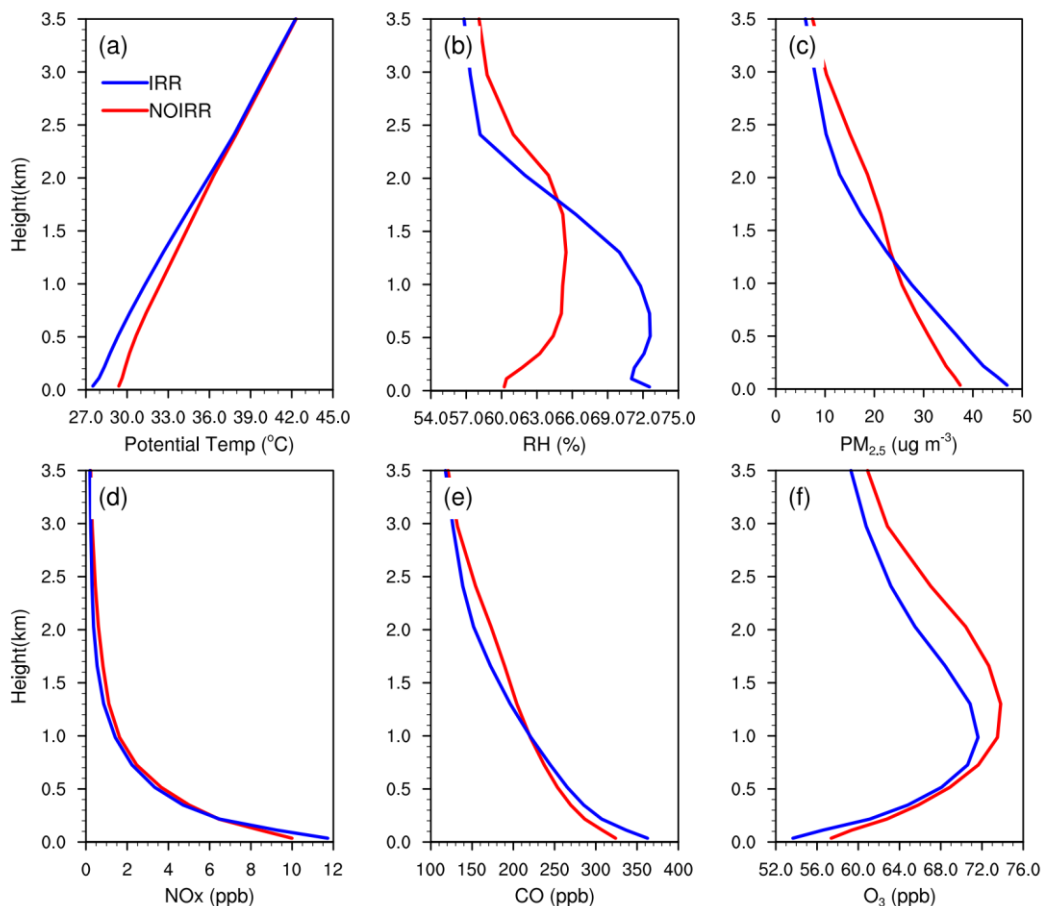
323 **Figure 5. Diurnal cycles of (a, e)  $T_2$ , (b, f) RH, (c, g) 10 m wind speed, (d, h) PBLH from IRR and NOIRR in (a-d)**

324 **Puyang and (e-h) Chengdu during the summer of 2017.**

325

326





327

328 **Figure 6. Vertical profiles of daily mean (a) potential temperature (°C), (b) RH (%), (c) PM<sub>2.5</sub> (μg m<sup>-3</sup>), NO<sub>x</sub> (ppb),**

329 **CO (ppb) and O<sub>3</sub> (ppb) from IRR and NOIRR in Puyang during the summer of 2017.**

330

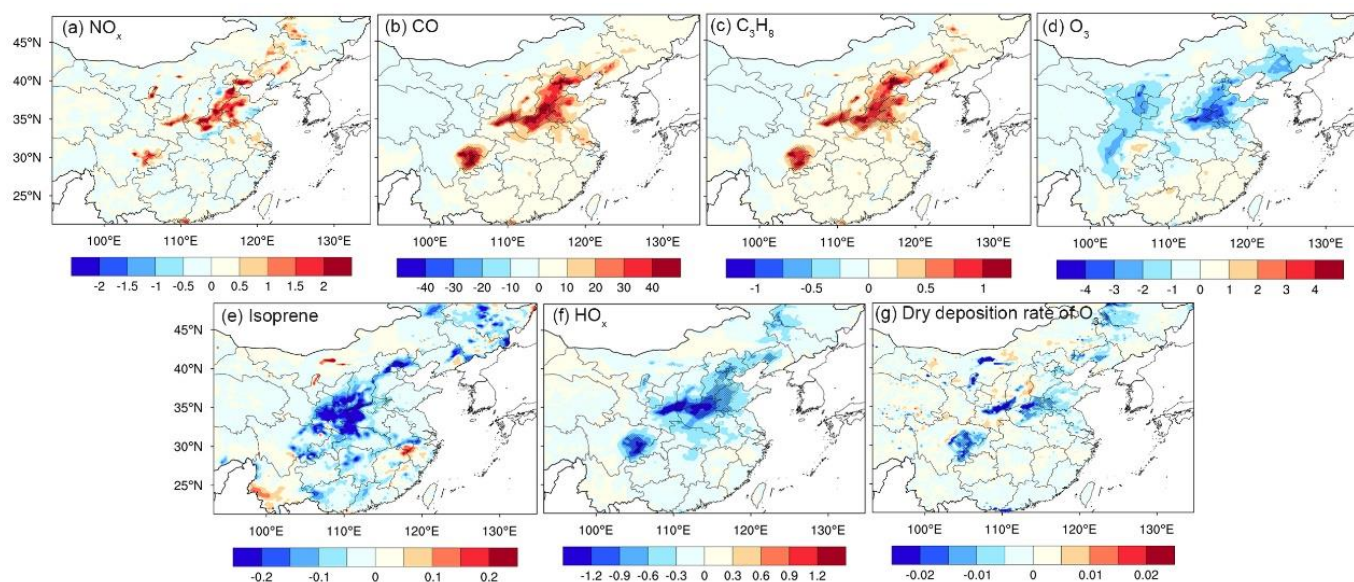
### 331 **3.3 Impacts of irrigation on gaseous pollutants**

332 The variations in meteorology may further modify the formation and fate of air pollutants. **Figure 7** demonstrates the  
 333 irrigation-induced changes in surface gaseous pollutants. The shallower atmospheric boundary layer and lower wind speed  
 334 induced by irrigation weaken the dispersion and trap primary pollutants in the PBL. Specifically, irrigation increases surface  
 335 NO<sub>x</sub> by 2 ppb, CO by 40 ppb, propane (C<sub>3</sub>H<sub>8</sub>) (a species of anthropogenic VOCs) by 1 ppb over irrigated areas in NCP and  
 336 SCB. However, the mean surface O<sub>3</sub> experiences an overall decline over the irrigated areas, with the largest decrease of 3–4



337 ppb occurring in northern Henan province. Such changes become smaller as the irrigated areas stretch to Hebei and Shandong  
 338 in NCP. The SCB, on the other hand, only witnesses a slight increase (0–2 ppb) in surface  $O_3$ , but the negative changes are  
 339 found in its surrounding regions and central China where irrigated areas are scarcely scattered. Moreover, irrigation reduces  
 340 atmospheric oxidation capacity, as evidenced by the decreases in oxidants ( $HO_x$ ) and  $O_3$ . Moreover, the dry deposition velocity  
 341 of  $O_3$  is also reduced in irrigated areas. Regarding the vertical profiles, irrigation increases  $O_3$  precursors including  $NO_x$  and  
 342 CO near the surface but decreases them above 1 km, while  $O_3$  is reduced greatly from surface to 3.5 km in Puyang, with a  
 343 reduction of 4 ppb near the surface (Fig. 6d–f). Irrigation lowers the altitude of maximum  $O_3$  by around 300 m. A similar  
 344 pattern is found in Chengdu, although the variation in  $O_3$  below 1 km is relatively small (Fig. S3d–f). Li et al. (2016) pointed  
 345 out that surface  $O_3$  has small variations in irrigated areas but rises by 2–7 ppb in surrounding non-irrigated areas in Central  
 346 Valley of California, which is different from our results. This discrepancy could be attributable to the more intensive irrigation  
 347 in their study, leading to stronger divergence and transport of  $O_3$  precursors to the surrounding areas.

348



349  
 350 **Figure 7. Same as Fig. 4 but for (a)  $NO_x$ , (b) CO, (c) propane ( $C_3H_8$ ), (d)  $O_3$ , (e) isoprene (ppb), (f)  $HO_x$  (ppt) and (g)**  
 351 **dry deposition velocity for  $O_3$  ( $cm\ s^{-1}$ ) during the summer of 2017.**

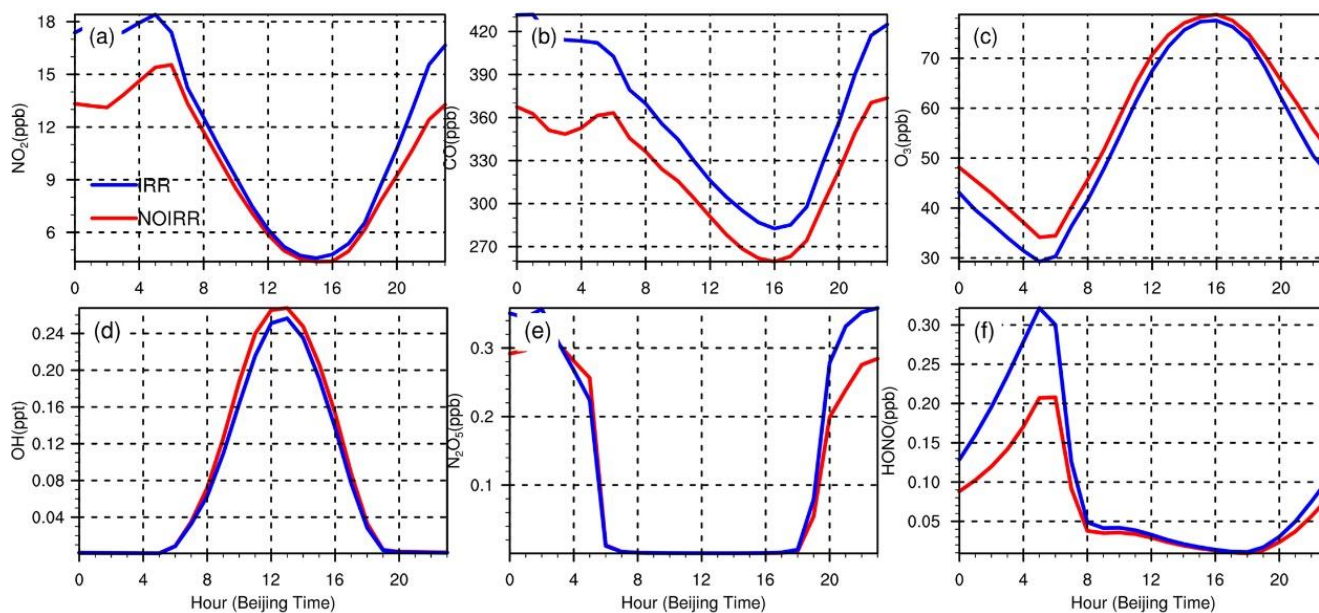
352



353 **Figure 8** exhibits the diurnal cycle of gaseous pollutants averaged over the summer. While irrigation has a stronger  
354 cooling effect in the afternoon, the most significant variations in these air pollutants occur at night with the increase of 4 and  
355 60 ppb in  $\text{NO}_2$  and CO, respectively. The reduction in surface  $\text{O}_3$  reaches a maximum of 5 ppb during 00:00–6:00 and minimum  
356 of 2 ppb in the afternoon. Some other secondary pollutants such as  $\text{N}_2\text{O}_5$  and HONO show drastic increases at night, implying  
357 a distinct nocturnal chemistry. For the most crucial oxidant, OH, which mainly appears at daytime in the presence of sunlight,  
358 the decrease due to irrigation reaches the peak at noon and is relatively smaller during morning and afternoon.

359 Meteorological variations play a significant role in tropospheric  $\text{O}_3$  formation and removal through natural emission  
360 pathways and chemical processes (Lu et al., 2019). Using models and observations, considerable research has suggested that  
361 temperature and RH are two principal factors influencing tropospheric  $\text{O}_3$ , but with opposite effects (e.g., Chen et al., 2019;  
362 Qian et al., 2022). Therefore, modified meteorology may influence the biogenic emissions, modulating photochemical  
363 production of  $\text{O}_3$  (Ren et al., 2022). However, we found that there is a small and insignificant reduction in isoprene in NCP  
364 and SCB, indicating its weak effect (Fig. 7e). Conversely, high water vapor has been found to enhance  $\text{O}_3$  loss via more  
365 complex pathways such as by participating in the formation of  $\text{HO}_x$  directly and slowing photochemical production via  
366 increasing cloud cover (Jacob and Winner, 2009; Han et al., 2020b). Moreover, since the reaction of  $\text{NO}_2 + \text{OH}$  is an important  
367 pathway for  $\text{O}_3$  removal in high- $\text{NO}_x$  environments (Wang et al., 2017), the elevated total  $\text{NO}_x$  concentration is likely  
368 responsible for daytime reduction of  $\text{O}_3$  and OH (Fig. 8). The NO titration might also be enhanced under high  $\text{NO}_x$   
369 concentration in IRR. At night, the elevated  $\text{NO}_2$  and RH promote the formation of  $\text{N}_2\text{O}_5$  and HONO through  $\text{O}_3$  oxidation and  
370  $\text{NO}_2$  hydrolysis, respectively, causing a drastic decline in  $\text{O}_3$  (Fig. 8c). Li et al. (2019) elucidated that reduction in  
371 heterogeneous uptake of  $\text{HO}_2$  onto aerosol surface because of the decrease in  $\text{PM}_{2.5}$  exacerbates  $\text{O}_3$  pollution in NCP. Thus, the  
372 increases in  $\text{PM}_{2.5}$  induced by irrigation may enhance the heterogeneous uptake process and hence slows down  $\text{O}_3$  production.  
373 Overall, we can exclude the influence of dry deposition rate of  $\text{O}_3$  given its reduction (Fig. 7g), which should have raised  $\text{O}_3$   
374 instead of lowering it, and the high  $\text{NO}_x$  due to weak mixing might be the major contributor to the reduction of  $\text{O}_3$  through  
375 oxidant titration ( $\text{NO} + \text{O}_3$  and  $\text{NO}_2 + \text{OH}$ ). Further research efforts are warranted to better understand and quantify the individual  
376 contributions of these processes to irrigation-induced  $\text{O}_3$  changes.

377



378

379 **Figure 8.** Same as Fig. 5 but for NO<sub>x</sub> (ppb), CO (ppb), O<sub>3</sub> (ppb), OH (ppt), N<sub>2</sub>O<sub>5</sub> (ppb), and HONO (ppb) in Puyang.

380

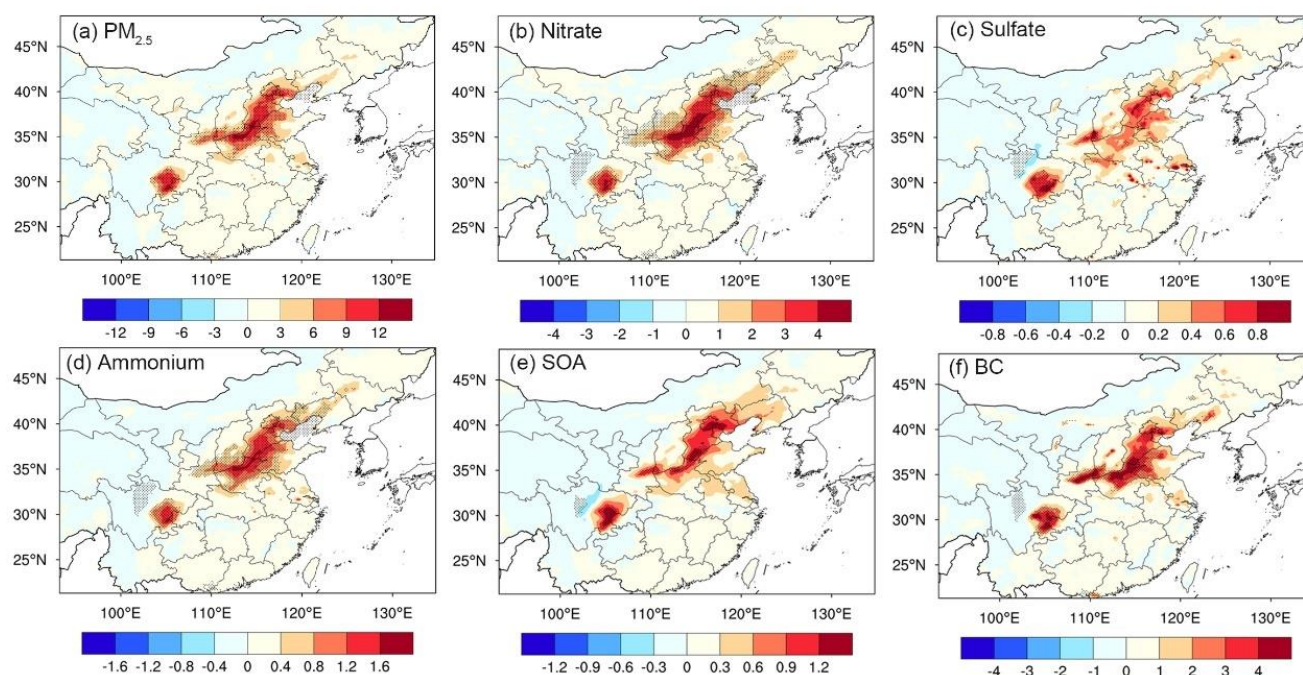
381 **3.4 Impacts of irrigation on PM<sub>2.5</sub> and its components**

382 Meteorological conditions such as high RH, low PBLH and weak wind speed also play essential roles in facilitating the  
 383 accumulation and formation of PM<sub>2.5</sub> (Zhang et al., 2015; Chen et al., 2020). Particularly, humidity is positively correlated  
 384 with PM<sub>2.5</sub> in NCP due to the favorable conditions for aqueous-phase aerosol chemistry, while the correlation is negative in  
 385 the Pearl River Delta and Yangtze River Delta, given the dominant role of wet deposition in relation to precipitation in South  
 386 China (Wang et al., 2023; Zhai et al., 2019). **Figure 9** illustrates the differences of PM<sub>2.5</sub> and its components between IRR and  
 387 NOIRR. The corresponding relative percentage changes are shown in Fig. S4. Irrigation increases PM<sub>2.5</sub>, nitrate, sulfate,  
 388 ammonium, SOA and BC by around 12 (28 %), 4 (70 %), 0.6–0.8 (10–20 %), 1.2–1.6 (40 %), 1.2 (12–16 %) and 4 μg m<sup>-3</sup>  
 389 (15–20 %) in both NCP and SCB, respectively. Regarding the vertical profiles, PM<sub>2.5</sub> in Puyang and Chengdu mainly peaks at  
 390 47 and 58 μg m<sup>-3</sup> near the surface in IRR, respectively, approximately 9 and 6 μg m<sup>-3</sup> higher than that in NOIRR (Fig. 6c and  
 391 Fig. S3c). Notably, the RH at 60–80 %, which is also seen in IRR (Fig. 5b, f), favors multiphase chemistry (i.e., heterogeneous  
 392 and aqueous reactions) for secondary aerosol formation and hygroscopic growth, such as aqueous oxidation of SO<sub>2</sub>, aerosol



393 uptake of  $\text{NO}_2$ , heterogeneous uptake of  $\text{HO}_2$ , and  $\text{N}_2\text{O}_5$  hydrolysis (An et al., 2019; Tie et al., 2017; Sun et al., 2018). Therefore,  
 394 the increase in  $\text{PM}_{2.5}$  components above is the total contribution from physical and chemical processes. It should be noted that  
 395 the increase in SOA is primarily due to physical processes, because SOA formulation in our model is only related to CO,  
 396 isoprene and other VOC emissions with no detailed SOA chemistry.

397



398

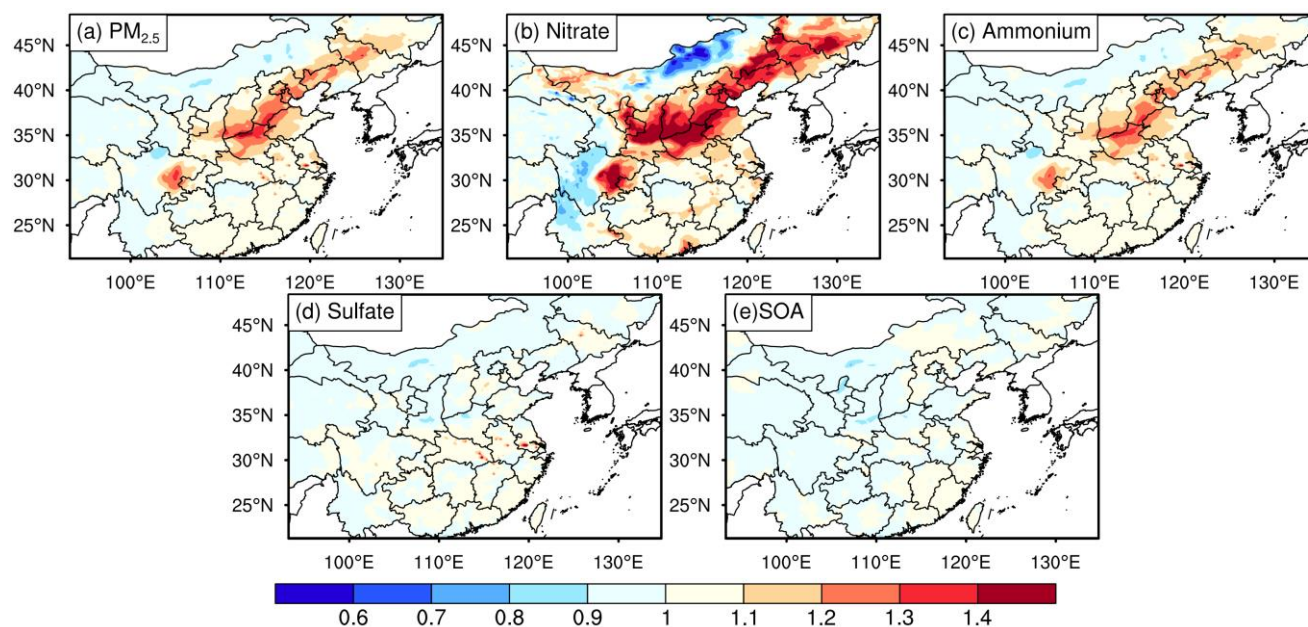
399 **Figure 9. Same as Fig. 4 but for (a)  $\text{PM}_{2.5}$ , (b) nitrate, (c) sulfate, (d) ammonium, (e) SOA and (f) BC ( $\mu\text{g m}^{-3}$ ).**

400

401 To examine the contribution of chemical processes, we followed the approach of Huang et al. (2021) using the ratio of  
 402 secondary  $\text{PM}_{2.5}$  (i.e., nitrate, sulfate, ammonium, SOA) versus BC between IRR and NOIRR, i.e.,  
 403  $(\text{PM}_{2.5}/\text{BC})_{\text{IRR}}/(\text{PM}_{2.5}/\text{BC})_{\text{NOIRR}}$  (Fig. 10). The basis is that BC is a primary aerosol and the changes in BC induced by irrigation  
 404 can be approximately regarded as the contribution of physical processes. Thus, aerosol formation is enhanced if the ratio is  
 405 larger than unity, while it is weakened if the ratio is below one. As shown in Fig. S4, the relative increases in BC are around  
 406 15–20 % (i.e., contribution from physical process). Secondary formation of  $\text{PM}_{2.5}$  and ammonium are enhanced over NCP and



407 SCB with the ratio ranging from 1.1 to 1.3 (Fig. 10a, c). Sulfate can be generated from the gas-phase oxidation of SO<sub>2</sub> by OH  
 408 and aqueous oxidation by hydrogen peroxide (H<sub>2</sub>O<sub>2</sub>) and O<sub>3</sub>. The ratio, which is close to one, suggested that the formation of  
 409 sulfate is less evident and even suppressed (Fig. 10d), due to the decline in HO<sub>x</sub> and O<sub>3</sub> (Fig. 7). As expected, there is no  
 410 formation of SOA because of the lack of detailed SOA chemistry in response to irrigation (Fig. 10e). By comparing the  
 411 differences in the relative changes in secondary aerosols and BC between IRR and NOIRR (i.e., subtracting the fractional  
 412 changes in BC from the fractional changes in other aerosol species), we can approximately estimate the contribution of  
 413 secondary formation to the increases in PM<sub>2.5</sub> (Fig. S5), which is around 5–10 %, ~ 60 %, 10–30 % to the total increase in  
 414 PM<sub>2.5</sub>, nitrate, and ammonium, respectively, while it is negligible for sulfate and SOA.  
 415



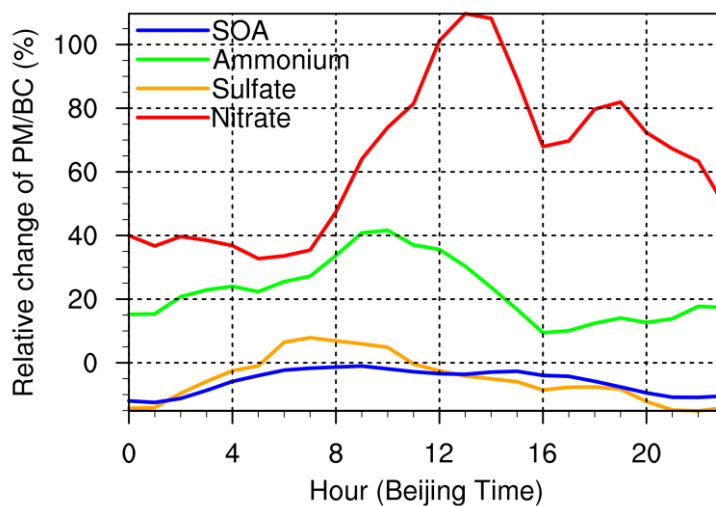
416  
 417 **Figure 10. Spatial distribution of the ratio of (a) PM<sub>2.5</sub> and (c–f) secondary PM<sub>2.5</sub> (sulfate, nitrate, ammonium and SOA)**  
 418 **versus BC between the IRR and NOIRR, i.e.  $(PM_{2.5}/BC)_{IRR}/(PM_{2.5}/BC)_{NOIRR}$  during the summer of 2017.**

419  
 420 **Figure 11** demonstrates the diurnal cycle of relative changes in PM<sub>2.5</sub> due to secondary formation induced by irrigation at  
 421 Puyang. Nitrate formation remains at a high level during daytime, with two peaks occurring at 13:00 and 19:00, respectively,



422 while it is relatively lower during nighttime. The enhanced production throughout the day suggests the dominance of the  
423 reaction of daytime  $\text{NO}_2 + \text{OH}$  and nighttime  $\text{N}_2\text{O}_5$  hydrolysis, which are two major formation pathways for nitrate (Alexander  
424 et al., 2020). This is supported by the drastic increase in  $\text{N}_2\text{O}_5$  during nighttime and the decline in OH during daytime, driven  
425 by the elevated concentration of  $\text{NO}_2$  in IRR (Fig. 8). Apart from the chemical production, the cooling effect of irrigation  
426 during daytime can inhibit the transition of nitrate from particle to gas phase, which reduces the nitrate loss and is another  
427 possible driver for the drastic increase in nitrate during daytime. Moreover, the increase in HONO indicates its essential  
428 contribution through  $\text{NO}_2$  hydrolysis to form  $\text{HNO}_3$  and HONO at high  $\text{NO}_x$  levels (Fig. 8f, Xue et al., 2014, Alexander et al.,  
429 2020). Ammonium formation follows a similar trend to nitrate, with the maximum ratio reaching 40 % at daytime, because of  
430 the neutralization of  $\text{HNO}_3$  by  $\text{NH}_3$  to form ammonium nitrate. In general, irrigation enhances formation of nitrate and  
431 ammonium by lowering temperature and raising humidity. The contribution of the chemical pathways is almost triple that of  
432 physical process for nitrate, but comparable for ammonium and  $\text{PM}_{2.5}$ . The production of SOA and sulfate is not sensitive to  
433 irrigation. The enhancement of nitrate formation through the  $\text{NO}_2 + \text{OH}$  and  $\text{N}_2\text{O}_5$  hydrolysis in IRR is well coinciding with the  
434 reduction in  $\text{O}_3$  and OH during daytime and nighttime as discussed in Sect. 3.3, respectively.

435



436

437 **Figure 11. Diurnal cycle of the relative changes (%) in the ratio of secondary  $\text{PM}_{2.5}$  components versus BC in IRR**  
438 **relative to NOIRR in Puyang during the summer of 2017.**



439

### 440 **3.5 Emission control strategies to alleviate the deterioration of PM<sub>2.5</sub> pollution by irrigation**

441 Reducing nitrate is becoming a priority in China in recent years, as it dominates the chemical composition of PM<sub>2.5</sub> in  
442 eastern China and shows relatively smaller decline compared with the total PM<sub>2.5</sub> since the implementation of stringent  
443 emission control strategy in 2013 (Zhai et al., 2021; Sun et al., 2022). Through the above analysis, we found that irrigation  
444 increases nitrate and ammonium, which makes it even more challenging to reduce nitrate pollution. However, given that  
445 irrigation has been shown to mitigate both water stress and heat stress experienced by crops, and has been viewed as an  
446 effective way to buffer yield losses caused by future climate change (Abramoff et al., 2023; Liao et al., 2024), it is important  
447 to explore the suitable emission reduction strategies to alleviate nitrate pollution while keeping these irrigation benefits.  
448 Therefore, we designed four extra sensitivity experiments with 20 %, 50 % combined emission reduction in NO<sub>x</sub> and NH<sub>3</sub>,  
449 50 % individual emission reduction of NO<sub>x</sub> and NH<sub>3</sub>. The effects of emission reductions can be estimated by comparing the  
450 extra sensitivity experiments with IRR, while the combined effects of both emission reductions and irrigation can be derived  
451 by comparing them with NOIRR. **Figure 12** exhibits the irrigation benefits and relative changes in nitrate and ammonium  
452 under different emission scenarios along with irrigation. Irrigation raises regional averaged nitrate by ~ 40 and 30 % over NCP  
453 and SCB, respectively, in comparison to NOIRR. The 20 % combined emission reductions in NH<sub>3</sub> and NO<sub>x</sub> effectively offset  
454 the irrigation-induced increase in nitrate in both regions, and the reduction in nitrate caused by 50 % combined reduction even  
455 doubles that increase in IRR. However, individual emission reductions in NO<sub>x</sub> and NH<sub>3</sub> by up to 50 % only has half benefit  
456 compared with 50 % combined reduction, implying the needs for synergistic control of air pollution. Changes in ammonium  
457 are similar to those in nitrate except that it needs 50% individual emission reductions in NO<sub>x</sub> or NH<sub>3</sub> to totally offset the  
458 ammonium increase in IRR over both regions.

459 Notably, although 50% combined and individual emission reductions in NH<sub>3</sub> and NO<sub>x</sub> can strongly reduce nitrate and  
460 ammonium, the increase in nighttime O<sub>3</sub> due to weakened titration effect in large city clusters including the Beijing-Tianjin-  
461 Hebei (BTH) region, Yangtze River delta and Pearl River Delta should be recognized, while the decrease in O<sub>3</sub> dominates the  
462 rest of other regions, reflecting nonlinear responses (Fig. S6). **Figure 13** further shows the corresponding responses of O<sub>3</sub>.

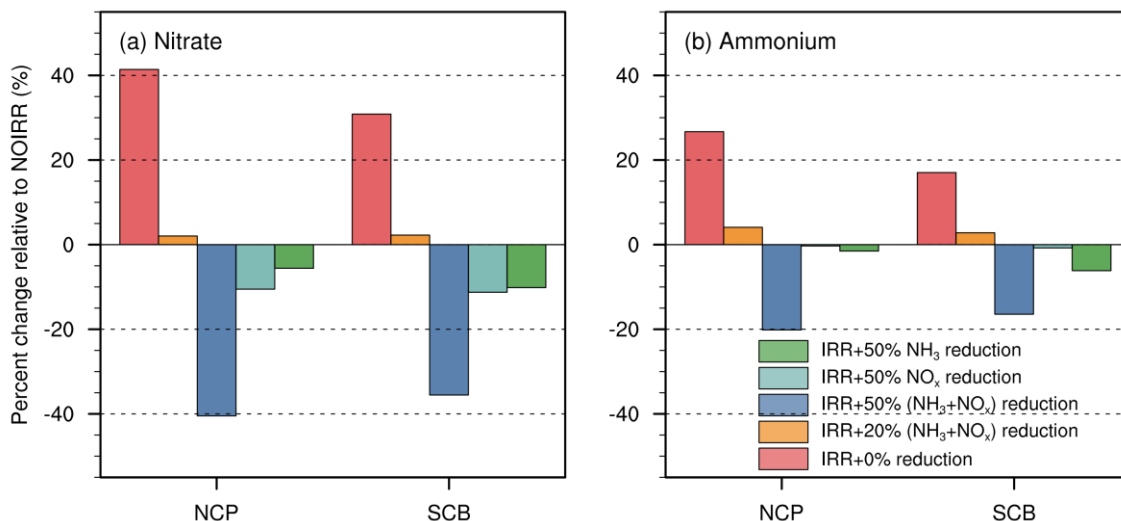




463 Taking BTH as an example, the 3.2 % reduction in nighttime  $O_3$  induced by irrigation is largely offset by 20% combined  
464 emission reductions. In other words, irrigation totally counteracts the rise in nighttime  $O_3$  due to  $NO_x$  reduction. Regarding the  
465 50% combined and individual emission reduction, irrigation only cancels out by 66–74 % of  $O_3$  increase (Fig. 13a). By contrast,  
466 the 50% combined and individual emission reductions in  $NO_x$  reduce daytime  $O_3$  by 0.5 % and irrigation further raises this  
467 benefit to 3 % (Fig. 13b). Even though 20 % combined reduction raises daytime  $O_3$  by 1.6 %, irrigation fully reverses this  
468 situation, leading to a net decrease by 0.9 %. For daily average  $O_3$ , irrigation still completely counteracts the  $O_3$  increase in all  
469 scenarios except the 50 % individual reduction of  $NH_3$ , with the contribution of 108–140 % (Fig. 13c). The 50 % individual  
470 reduction of  $NH_3$  results in the largest increase in daytime  $O_3$  (4.3 %) among all experiments due to less neutralization with  
471  $HNO_3$ , exceeding the irrigation benefits (–2.5 %) (Fig. 13b). Similar changes in daytime, nighttime and daily mean  $O_3$  are also  
472 seen in the whole NCP (Fig. 13d–e), except that irrigation benefits (–3.6 %) exceeds the nighttime  $O_3$  increases (2.6 %) due  
473 to emission reductions in the four scenarios (Fig. 13d). In SCB, almost all emission reduction strategies reduce surface  $O_3$   
474 substantially, regardless of daytime and nighttime, which is larger than irrigation-induced reduction in  $O_3$ . It is worthwhile  
475 noting that 50 % combined emission reduction and individual reduction of  $NO_x$  are the most effective in this region, followed  
476 by 20 % combined emission reduction and only controlling  $NH_3$  emission has the least efficiency.

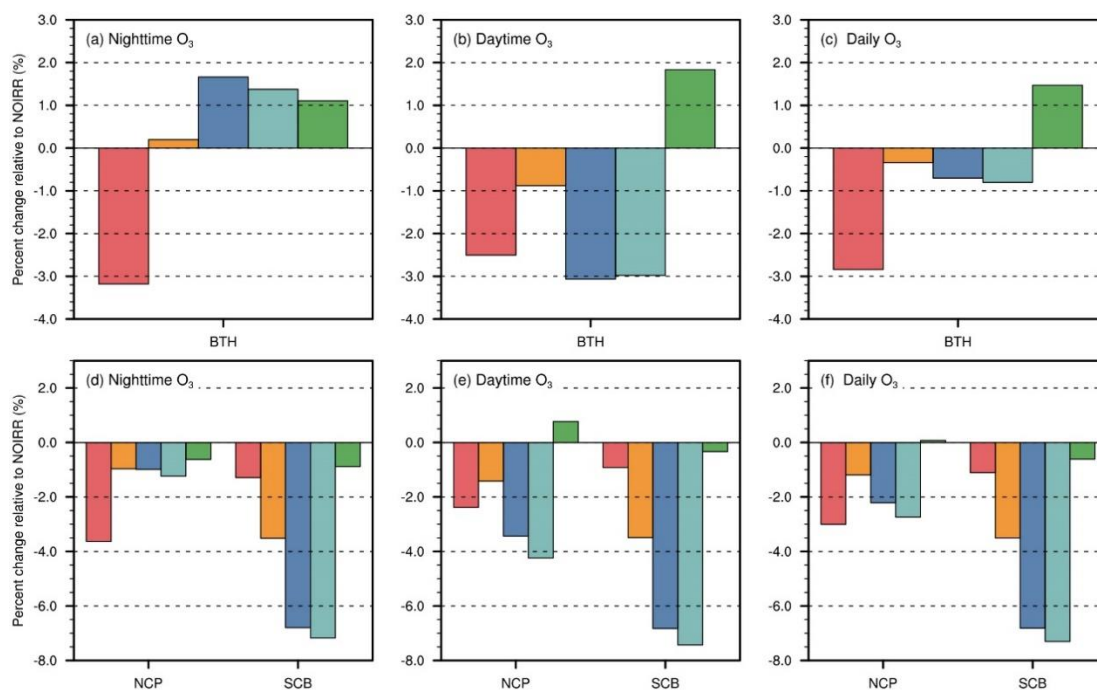
477 Overall, we found that 20 % combined emission reductions in  $NH_3$  and  $NO_x$  is an effective and feasible way to buffer the  
478 adverse effects of irrigation on nitrate and ammonium in NCP and SCB, while leading to the smallest increase in nighttime  $O_3$   
479 (only 0.2 %) in BTH. Although 50 % combined emission reductions are more effective in reducing ammonium nitrate, it can  
480 lead to an increase in nighttime  $O_3$  by 1.6 % that irrigation can only offset by 66 %. Our results are similar to previous modeling  
481 studies in which  $PM_{2.5}$  shows nonlinear responses to emission reductions and the combined emission reductions of precursors  
482 are more beneficial for nitrate reduction (Cheng et al., 2019; Zhai et al., 2021; Liu et al., 2021c).

483



484

485 **Figure 12. Percent changes in (a) nitrate and (b) ammonium in response to IRR with 0, 20, 50 % combined emission**  
 486 **reductions in NH<sub>3</sub> and NO<sub>x</sub>, and 50 % individual emission reduction in NH<sub>3</sub> and NO<sub>x</sub>, relative to NOIRR, averaged**  
 487 **over NCP and SCB during the summer of 2017.**



488

489 **Figure 13. Same as Fig.12 but for nighttime, daytime and daily mean surface O<sub>3</sub> in Beijing-Tianjin-Hebei (BTH), NCP**  
 490 **and SCB.**



#### 491 **4 Conclusions and discussion**

492 China possesses the largest irrigated area of the world and the expanding irrigated area has driven changes in many aspects  
493 of socioeconomic and environmental concerns, including in energy use and its related CO<sub>2</sub> emissions, water resources,  
494 terrestrial emissions of pollutants and greenhouse gases (N<sub>2</sub>O and CH<sub>4</sub>), and regional climate (Yang et al., 2023). All of these  
495 would alter regional air quality through influencing emissions, transport and mixing, chemistry and deposition. To reveal the  
496 underlying mechanisms, we employed the WRF-GC model, which incorporates comprehensive ozone–NO<sub>x</sub>–VOC–aerosol  
497 chemistry, to investigate the effects of irrigation on air pollution in China, with a particular focus on the intensively irrigated  
498 and polluted NCP and SCB. The model generally captures the regions characterized by high levels of PM<sub>2.5</sub> and O<sub>3</sub> pollution,  
499 including NCP and SCB. By analyzing the simulations with and without irrigation, we found that irrigation raises soil moisture,  
500 surface humidity and cloud cover, but reduces surface air temperature and PBLH. The weakened turbulence and shallow  
501 boundary layer further increase primary air pollutants including CO and NO<sub>x</sub> by 40 and 2 ppb, respectively, over irrigated  
502 areas. However, irrigation greatly reduces nighttime and daily mean O<sub>3</sub> by 5 and 3–4 ppb averaged over NCP, respectively,  
503 around five times the value in previous study focusing on Central Valley of California. Such reductions are attributable to the  
504 enhancement of oxidant titration at elevated NO<sub>x</sub> concentration, although other mechanisms, such as enhanced O<sub>3</sub> hydrolysis  
505 with high atmospheric water vapor, as well as slow photochemical reactions because of low temperature and high cloud cover,  
506 and heterogeneous uptake of HO<sub>2</sub>, might play some roles as well.

507 PM<sub>2.5</sub> shows complex sensitivities to meteorological changes due to its various components. Specifically, irrigation-  
508 induced high RH promotes nitrate formation through three major pathways, i.e., NO<sub>2</sub>+OH, NO<sub>2</sub> and N<sub>2</sub>O<sub>5</sub> hydrolysis. Strong  
509 cooling at daytime also suppresses the transition of nitrate from the particle to gas phase and thus reduces the nitrate loss.  
510 Ammonium is also enhanced through the neutralization of NH<sub>3</sub> with HNO<sub>3</sub>, since high RH and low temperature facilitate the  
511 partitioning of gases to particles. By contrast, weak atmospheric oxidation capacity due to irrigation suppresses sulfate  
512 formation. Another important finding is that both weak dispersion and secondary formation increase PM<sub>2.5</sub>, nitrate, sulfate,  
513 ammonium, SOA and BC by 12 (28 %), 4 (70 %), 0.6–0.8 (10–20 %), 1.2–1.6 (40 %), 1.2 (12–16 %) and 4 μg m<sup>-3</sup> (15–20 %),  
514 respectively, among which physical processes contribute approximately 15–20 %, whereas secondary chemical formation  
515 accounts for 5–10 %, ~ 60 %, and 10–30 % of the overall increase in PM<sub>2.5</sub>, nitrate and ammonium, respectively. In order to



516 alleviate the increase in  $PM_{2.5}$  in intensively irrigated areas, we further conducted several sensitivity experiments, which  
517 suggested that the 20 % combined emission reductions in  $NH_3$  and  $NO_x$  can effectively offset the negative effects of irrigation  
518 on  $PM_{2.5}$  nitrate without worsening nighttime  $O_3$  pollution in large city clusters.

519 The expansion of irrigated areas in China has slowed down since the 1980s and the IWU declines from the mid-1990s to  
520 the early 2000s, because of the advancement of irrigation systems such as sprinkler and drip irrigation (Zhou et al., 2020; Han  
521 et al., 2020a). However, the trend was reversed to a slight increase again since 2011 in water-scarce regions including NCP,  
522 primarily driven by cropland expansion (Qi et al., 2022; Zhang et al., 2022). It is projected that the IWU in China will increase  
523 by 8.5–17.1 % and 6.8–34.8 % by the 2050s and 2100s, respectively, under various warming scenarios (Liu et al., 2024a). This  
524 corresponds to the paradox of irrigation efficiency (Grafton et al., 2018), in which water conserved from high-efficient  
525 irrigation methods would be used for irrigation expansion to maximize crop yields and farmers' revenues, with government  
526 subsidies for modern irrigation systems (Zhang et al., 2022). Therefore, the increasing adoption of water-saving irrigation  
527 systems in the future may potentially decrease surface water vapor and increase surface temperature and PBLH, as evidenced  
528 by our previous work (Yuan et al., 2023). These changes are favorable for aerosol dissipation, conversion of nitrate to gas  
529 phase and suppression of nitrate formation, but they may contribute to  $O_3$  formation, in contrast with the present-day situation  
530 of widespread traditional irrigation. Consequently, the proposed emission control strategy for nitrate mitigation here is likely  
531 to exacerbate  $O_3$  pollution, which cannot be offset by irrigation. Thus, future emission control strategies may prioritize  $O_3$   
532 mitigation (e.g., through reducing VOCs emissions) during the transition from conventional irrigation methods to water-saving  
533 irrigation techniques. In other words, a tradeoff between air pollution control and irrigation needs has to be carefully considered  
534 in the future.

535 We note that all these results discussed above are based on one summer simulation because of the demanding computer  
536 resources required by WRF-GC model, and the effects of irrigation can have interannual variability (Sorooshian et al., 2012;  
537 Li et al., 2016). Conducting long-term simulations will provide a more comprehensive assessment of these effects. Indeed, we  
538 have conducted long-term simulations using WRF-only model in our previous work and found that long-term effects of  
539 irrigation on meteorology are similar to those reported in this study, likely reflecting the summer of 2017 being rather normal  
540 in terms of climate conditions. Thus, we expect that the interannual variability of climate may not significantly interfere with



541 our results regarding atmospheric chemistry. However, we could not quantitatively show which pathway dominates the decrease  
542 in  $O_3$  and increase in  $PM_{2.5}$ , given that the standard WRF-GC model cannot diagnose individual chemical pathways, so  
543 perturbation experiments or tagged simulations are promising for addressing this issue in future work. Moreover, the model  
544 uncertainty in simulating the composition of  $PM_{2.5}$  should be recognized, as Travis et al. (2022) found that GEOS-Chem  
545 overestimates nitrate by 36 % due to the missing sink of  $HNO_3$ .

546 Overall, this study represents the first work to gain an insight into the possible range of air quality outcomes arising from  
547 irrigation over China. Our findings indicate the nonnegligible and contrasting effects of irrigation on  $PM_{2.5}$  and  $O_3$ , and  
548 emphasize the roles of changing irrigation practices in mitigating regional air pollution, suggesting that a coordinated approach  
549 is needed to simultaneously address air pollution control, water conservation, climate change adaption and food security. This  
550 study not only informs policymakers how to design emission control strategies and land management for air pollution control  
551 in intensively irrigated and heavily polluted regions, but also encourages farmers to adopt sustainable farming practices to  
552 maximize their socioeconomic gains. All of these contribute to the multiple Sustainable Development Goals (SDGs) including  
553 Goal 2 “Zero Hunger”, Goal 3 “Good Health and Well-being”, Goal 6 “Clean Water and Sanitation”, and Goal 13 “Climate  
554 Action”. For example, using water-saving irrigation systems in place of traditional ones can raise crop yields, alleviate water  
555 scarcity, and reduce  $PM_{2.5}$  pollution, but with a possible worsening of in  $O_3$  pollution, which may then have to be mitigated by  
556 tighter VOC emission control measures. On the other hand, as  $O_3$  control has been suggested to be more beneficial for  
557 safeguarding food security than  $PM_{2.5}$  control (Liu et al., 2024b), irrigation itself may serve as a potential approach to not only  
558 protect crops from water and heat stresses directly, but also alleviate  $O_3$  exposure and its damage via modulating atmospheric  
559 chemistry indirectly. Achieving these various SDGs requires multi-sectoral collaboration, and our study provides a valuable  
560 reference for decision making in this regard.

### 561 **Data availability**

562 The WRF-GC model coupled with irrigation schemes is now available from <https://wrfgc.readthedocs.io/en/latest/> (last access:  
563 1 May 2024). Model output data are available upon request.

564



565 **Competing interests**

566 The contact author has declared that neither they nor their co-authors have any competing interests. At least one of the  
567 (co-)authors is a member of the editorial board of Atmospheric Chemistry and Physics.

568 **Author contribution:**

569 APKT conceived the study and revised this manuscript. TY coupled the irrigation schemes into WRF-GC, performed the  
570 simulations and analysis as well as wrote the manuscript draft. AZ and MF give suggestions on how to use WRF-GC model.  
571 DHYY helped design model experiments. TMF, JW and SL reviewed and edited the manuscript.

572 **Acknowledgments**

573 This work was supported by the General Research Fund (project no.: 14307722) granted by the Research Grants Council (RGC)  
574 to APKT, funding from the State Key Laboratory of Agrobiotechnology and Innovation and Technology Commission (project  
575 no.: 8300031, 8300036, 8300070) granted to APKT and JW, National Natural Science Foundation of China (project no.:  
576 31922090) granted to JW, and Hong Kong Ph.D. Fellowship granted by RGC to TY.

577 **References**

- 578 Abramoff, R. Z., Ciais, P., Zhu, P., Hasegawa, T., Wakatsuki, H., and Makowski, D.: Adaptation strategies strongly reduce the  
579 future impacts of climate change on simulated crop yields, *Earth's Future*, 11, e2022EF003190,  
580 <https://doi.org/10.1029/2022EF003190>, 2023.
- 581 Alexander, B., Sherwen, T., Holmes, C. D., Fisher, J. A., Chen, Q., Evans, M. J., and Kasibhatla, P.: Global inorganic nitrate  
582 production mechanisms: comparison of a global model with nitrate isotope observations, *Atmos. Chem. Phys.*, 20, 3859–  
583 3877, <https://doi.org/10.5194/acp-20-3859-2020>, 2020.
- 584 An, Z., Huang, R. J., Zhang, R., Tie, X., Li, G., Cao, J., Zhou, W., Shi, Z., Han, Y., Gu, Z., and Ji, Y.: Severe haze in northern  
585 China: A synergy of anthropogenic emissions and atmospheric processes, *Proc. Natl. Acad. Sci. U.S.A.*, 116(18), 8657–  
586 8666, <https://doi.org/10.1073/pnas.1900125116>, 2019.
- 587 Bavi, A., Kashkuli, H. A., Boroomand, S., Naseri, A., and Albaji, M.: Evaporation losses from sprinkler irrigation systems  
588 under various operating conditions, *Journal of Applied Sciences*, 9(3), 597–600, <https://doi.org/10.3923/jas.2009.597.600>,  
589 2009.
- 590 Beguería, S., Vicente-Serrano, S. M., and Angulo-Martínez, M. A.: Multiscalar global drought dataset: the SPEIbase: a new



- 591 gridded product for the analysis of drought variability and impacts, *Bull. Am. Meteorol. Soc.*, 91, 1351–1356,  
592 <https://doi.org/10.1175/2010bams2988.12010>.
- 593 Chen, Z., Chen, D., Zhao, C., Kwan, M.-p., Cai, J., Zhuang, Y., Zhao, B.o., Wang, X., Chen, B., Yang, J., Li, R., He, B., Gao,  
594 B., Wang, K., and Xu, B.: 2020. Influence of meteorological conditions on PM<sub>2.5</sub> concentrations across China: a review  
595 of methodology and mechanism, *Environ. Int.* 139, 105558, <https://doi.org/10.1016/j.envint.2020.105558>, 2020.
- 596 Chen, Z.Y., Zhuang, Y., Xie, X., Chen, D., Cheng, N., Yang, L., and Li, R.: Understanding long-term variations of  
597 meteorological influences on ground ozone concentrations in Beijing during 2006–2016, *Environ. Pollut.*, 245, 29–37,  
598 <https://doi.org/10.1016/j.envpol.2018.10.117>, 2019.
- 599 Cheng, J., Su, J., Cui, T., Li, X., Dong, X., Sun, F., Yang, Y., Tong, D., Zheng, Y., Li, Y., Li, J., Zhang, Q., and He, K.: Dominant  
600 role of emission reduction in PM<sub>2.5</sub> air quality improvement in Beijing during 2013–2017: a model-based decomposition  
601 analysis, *Atmos. Chem. Phys.*, 19, 6125–6146, <https://doi.org/10.5194/acp-19-6125-2019>, 2019.
- 602 Cook, B., Shukla, S. P., Puma, M. J., and Nazarenko, L. S.: Irrigation as an historical climate forcing, *Clim. Dyn.*, 44, 1715–  
603 1730, <https://doi.org/10.1007/s00382-014-2204-7>, 2015.
- 604 Currell, M.J., Han, D., Chen, Z., and Cartwright, I.: Sustainability of groundwater usage in northern China: dependence on  
605 palaeowaters and effects on water quality, quantity and ecosystem health, *Hydrol. Processes*, 26, 4050–4066.  
606 <https://doi.org/10.1002/hyp.9208>, 2012.
- 607 Dang, R., Liao, H., and Fu, Y.: Quantifying the anthropogenic and meteorological influences on summertime surface ozone in  
608 China over 2012–2017, *Sci. Total Environ.*, 754, 142394, <https://doi.org/10.1016/j.scitotenv.2020.142394>, 2021.
- 609 Deng, C., Tian, S., Li, Z., and Li, K.: Spatiotemporal characteristics of PM<sub>2.5</sub> and ozone concentrations in Chinese urban  
610 clusters, *Chemosphere*, 295, 133813, <https://doi.org/10.1016/j.chemosphere.2022.133813>, 2022.
- 611 Feng, X., Lin, H., Fu, T.-M., Sulprizio, M. P., Zhuang, J., Jacob, D. J., Tian, H., Ma, Y., Zhang, L., Wang, X., Chen, Q., and  
612 Han, Z.: WRF-GC (v2.0): online two-way coupling of WRF (v3.9.1.1) and GEOS-Chem (v12.7.2) for modeling regional  
613 atmospheric chemistry–meteorology interactions, *Geosci. Model Dev.*, 14, 3741–3768, <https://doi.org/10.5194/gmd-14-3741-2021>, 2021.
- 615 Guenther, A. B., Jiang, X., Heald, C. L., Sakulyanontvittaya, T., Duhl, T., Emmons, L. K., and Wang, X.: The Model of  
616 Emissions of Gases and Aerosols from Nature version 2.1 (MEGAN2.1): an extended and updated framework for  
617 modeling biogenic emissions, *Geosci. Model Dev.*, 5, 1471–1492, <https://doi.org/10.5194/gmd-5-1471-2012>, 2012.
- 618 Grafton, R. Q., Williams, J., Perry, C. J., Molle, F., Rihler, C., Steduto, P., Udall, B., Wheeler, S. A. Wang, Y., Garrick, D.,  
619 and Allen, R. G.: The paradox of irrigation efficiency, *Science*, 361(6404), 748–750.  
620 <https://doi.org/10.1126/science.aat9314>, 2018.
- 621 Han, S., Tian, F., and Gao, L.: Current status and recent trend of irrigation water use in China, *Irrig. Drain.*, 69, 25–35.  
622 <https://doi.org/10.1002/ird.2441>, 2020a.
- 623 Han, H., Liu, J., Shu, L., Wang, T., and Yuan, H.: Local and synoptic meteorological influences on daily variability in  
624 summertime surface ozone in eastern China, *Atmos. Chem. Phys.*, 20, 203–222, <https://doi.org/10.5194/acp-20-203-2020>,  
625 2020b.
- 626 He, C., Valayamkunnath, P., Barlage, M., Chen, F., Gochis, D., Cabell, R., Schneider, T., Rasmussen, R., Niu, G.-Y., Yang, Z.-  
627 L., Niyogi, D., and Ek, M.: The Community Noah-MP Land Surface Modeling System Technical Description Version 5.0.



- 628 NCAR Technical Note, NCAR/TN-575+STR, <https://doi.org/10.5065/ew8g-yr95>, 2023.
- 629 Hodzic, A. and Jimenez, J. L.: Modeling anthropogenically controlled secondary organic aerosols in a megacity: a simplified  
630 framework for global and climate models, *Geosci. Model Dev.*, 4, 901–917, <https://doi.org/10.5194/gmd-4-901-2011>,  
631 2011.
- 632 Huang, R.J., Zhang, Y., Bozzetti, C., Ho, K. F., Cao, J. J., Han, Y., Daellenbach, K. R., Slowik, J. G., Platt, S. M., Canonaco,  
633 F., Zotter, P., Wolf, R., Pieber, S. M., Bruns, E. A., Crippa, M., Ciarelli, G., Piazzalunga, A., Schwikowski, M., Abbaszade,  
634 G., Schnelle-Kreis, J., Zimmermann, R., An, Z., Szidat, S., Baltensperger, U., Haddad, I. E., Prévôt, A. S. h.: High  
635 secondary aerosol contribution to particulate pollution during haze events in China, *Nature*, 514, 218–222,  
636 <https://doi.org/10.1038/nature13774>, 2014.
- 637 Huang, X., Ding, A., Gao, J., Zheng, B., Zhou, D., Qi, X., Tang, R., Wang, J., Ren, C., Nie, W., Chi, X., Xu, Z., Chen, L., Li,  
638 Y., Che, F., Pang, N., Wang, H., Tong, D., Qin, W., Cheng, W., Liu, W., Fu, Q., Liu, B., Chai, F., Davis, S., Zhang, Q., and  
639 He, K.: Enhanced secondary pollution offset reduction of primary emissions during COVID-19 lockdown in China, *Natl.*  
640 *Sci. Rev.*, 8(2), nwaal37, <https://doi.org/10.1093/nsr/nwaa137>, 2021.
- 641 Hudman, R. C., Moore, N. E., Mebust, A. K., Martin, R. V., Russell, A. R., Valin, L. C., and Cohen, R. C.: Steps towards a  
642 mechanistic model of global soil nitric oxide emissions: implementation and space based-constraints, *Atmos. Chem. Phys.*,  
643 12, 7779–7795, <https://doi.org/10.5194/acp-12-7779-2012>, 2012.
- 644 IPCC, 2021: Climate Change 2021 - the Physical Science Basis, Contribution of Working Group I to the Sixth Assessment  
645 Report of the Intergovernmental Panel on Climate Change [Masson-Delmotte, V., P. Zhai, A. Pirani, S.L. Connors, C.  
646 Péan, S. Berger, N. Caud, Y. Chen, L. Goldfarb, M.I. Gomis, M. Huang, K. Leitzell, E. Lonnoy, J.B.R. Matthews, T.K.  
647 Maycock, T. Waterfield, O. Yelekçi, R. Yu, and B. Zhou (eds.)]. Cambridge University Press, In Press, Published: 9 August  
648 2021.
- 649 Iacono, M. J., Delamere, J. S., Mlawer, E. J., Shephard, M. W., Clough, S. A., and Collins, W. D.: Radiative forcing by longlived  
650 greenhouse gases: Calculations with the AER radiative transfer models, *J. Geophys. Res.-Atmos.*, 113, D13103,  
651 <https://doi.org/10.1029/2008JD009944>, 2008.
- 652 Jacob, D. J., and Winner, D. A.: Effect of climate change on air quality. *Atmos. Environ.*, 43(1), 51–63,  
653 <https://doi.org/10.1016/j.atmosenv.2008.09.051>, 2009.
- 654 Jacobson, M.: Short-term effects of agriculture on air pollutant and climate in California, *J. Geophys. Res.*, 113, D23101,  
655 <http://dx.doi.org/10.1029/2008JD010689>, 2008.
- 656 Jacobson, M.: Studying the effects of soil moisture on ozone, temperatures, and winds in Los Angeles, *J. Appl. Meteorol.*, 38,  
657 607–616, [http://dx.doi.org/10.1016/S1352-2310\(96\)00201-4](http://dx.doi.org/10.1016/S1352-2310(96)00201-4), 1999.
- 658 Jia, K., Liang, S. L., Wei, X. Q., Yao, Y. J., Yang, L. Q., Zhang, X. T., and Liu, D. Y.: Validation of Global Land Surface  
659 Satellite (GLASS) fractional vegetation cover product from MODIS data in an agricultural region, *Remote Sens. Lett.*, 9,  
660 847–856, <https://doi.org/10.1080/2150704X.2018.1484958>, 2018.
- 661 Kanamaru, H., and Kanamitsu, M.: Model diagnosis of nighttime minimum temperature warming during summer due to  
662 irrigation in the California Central Valley, *J. Hydrometeorol.*, 9, 1061–1072, <https://doi.org/10.1175/2008JHM967.1>, 2008.
- 663 Kim, P. S., Jacob, D. J., Fisher, J. A., Travis, K., Yu, K., Zhu, L., Yantosca, R. M., Sulprizio, M. P., Jimenez, J. L., Campuzano-  
664 Jost, P., Froyd, K. D., Liao, J., Hair, J. W., Fenn, M. A., Butler, C. F., Wagner, N. L., Gordon, T. D., Welti, A., Wennberg,





- 665 P. O., Crounse, J. D., St. Clair, J. M., Teng, A. P., Millet, D. B., Schwarz, J. P., Markovic, M. Z., and Perring, A. E.:  
666 Sources, seasonality, and trends of southeast US aerosol: an integrated analysis of surface, aircraft, and satellite  
667 observations with the GEOS-Chem chemical transport model, *Atmos. Chem. Phys.*, 15, 10411–10433,  
668 <https://doi.org/10.5194/acp-15-10411-2015>, 2015.
- 669 Lawston, P. M., Santanello Jr, J. A., Zaitchik, B. F., and Rodell, M.: Impact of irrigation methods on land surface model spinup  
670 and initialization of WRF forecasts, *J. Hydrometeorol.*, 16(3), 1135–1154, <https://doi.org/10.1175/JHM-D-14-0203.1>,  
671 2015.
- 672 Le, T., Wang, Y., Liu, L., Yang, J., Yung, Y. L., Li, G., and Seinfeld, J. H.: Unexpected air pollution with marked emission  
673 reductions during the COVID-19 outbreak in China, *Science*, 369(6504), 702–706,  
674 <https://doi.org/10.1126/science.abb7431>, 2020.
- 675 Lelieveld, J., Evans, J.S., Fnais, M., Giannadaki, D., and Pozzer, A.: The contribution of outdoor air pollution sources to  
676 premature mortality on a global scale, *Nature*, 525(7569), 367–371. <https://doi.org/10.1038/nature15371>, 2015.
- 677 Leung, D. M., Tai, A. P. K., Mickley, L. J., Moch, J. M., van Donkelaar, A., Shen, L., and Martin, R. V.: Synoptic meteorological  
678 modes of variability for fine particulate matter (PM<sub>2.5</sub>) air quality in major metropolitan regions of China, *Atmos. Chem.*  
679 *Phys.*, 18, 6733–6748, <https://doi.org/10.5194/acp-18-6733-2018>, 2018.
- 680 Leng, G., Leung, L. R., and Huang, M.: Significant impacts of irrigation water sources and methods on modeling irrigation  
681 effects in the ACME Land Model, *J. Adv. Model. Earth Syst.*, 9, 1665–1683, <https://doi.org/10.1002/2016MS000885>,  
682 2017.
- 683 Li, J., Mahalov, A., and Hyde, P.: Impacts of agricultural irrigation on ozone concentrations in the Central Valley of California  
684 and in the contiguous United States based on WRF-Chem simulations, *Agric. For. Meteorol.*, 221, 34–49,  
685 <https://doi.org/10.1016/j.agrformet.2016.02.004>, 2016.
- 686 Li, K., Jacob, D. J., Liao, H., Shen, L., Zhang, Q., and Bates, K. H.: Anthropogenic drivers of 2013–2017 trends in summer  
687 surface ozone in China, *Proc. Natl. Acad. Sci. U.S.A.*, 116(2), 422–427, <https://doi.org/10.1073/pnas.1812168116>, 2019.
- 688 Li, K., Jacob, D. J., Shen, L., Lu, X., De Smedt, I., and Liao, H.: Increases in surface ozone pollution in China from 2013 to  
689 2019: anthropogenic and meteorological influences, *Atmos. Chem. Phys.*, 20, 11423–11433, <https://doi.org/10.5194/acp-20-11423-2020>, 2020.
- 690
- 691 Li, M., Zhang, Q., Kurokawa, J.-I., Woo, J.-H., He, K., Lu, Z., Ohara, T., Song, Y., Streets, D. G., Carmichael, G. R., Cheng,  
692 Y., Hong, C., Huo, H., Jiang, X., Kang, S., Liu, F., Su, H., and Zheng, B.: MIX: a mosaic Asian anthropogenic emission  
693 inventory under the international collaboration framework of the MICS-Asia and HTAP, *Atmos. Chem. Phys.*, 17, 935–  
694 963, <https://doi.org/10.5194/acp-17-935-2017>, 2017a.
- 695 Li, M., Liu, H., Geng, G., Hong, C., Liu, F., Song, Y., Tong, D., Zheng, B., Cui, H., Man, H., Zhang, Q., and He, K.:  
696 Anthropogenic emission inventories in China: a review, *Natl. Sci. Rev.*, 4, 834–866, <https://doi.org/10.1093/nsr/nwx150>,  
697 2017b.
- 698 Li, X. L., Lu, H., Yu, L., and Yang, K.: Comparison of the spatial characteristics of four remotely sensed leaf area index  
699 products over China: Direct validation and relative uncertainties, *Remote Sens.*, 10, 26,  
700 <https://doi.org/10.3390/RS10010148>, 2018.
- 701 Liang, S., Cheng, J., Jia, K., Jiang, B., Liu, Q., Xiao, Z., Yao, Y., Yuan, W., Zhang, X., Zhao, X., & Zhou, J.: The global land



- 702 surface satellite (GLASS) product suite, *Bull. Am. Meteorol. Soc.*, 102 (2), E323–E337, [https://doi.org/10.1175/BAMS-](https://doi.org/10.1175/BAMS-D-18-0341.1)  
703 [D-18-0341.1](https://doi.org/10.1175/BAMS-D-18-0341.1), 2021.
- 704 Liao, D., Niu, J., Ciais, P., Du, T., Zhang, B., and Kang, S.: Changing climate threatens irrigation benefits of maize gross  
705 primary productivity in China, *Earth's Future*, 12, e2022EF003474, <https://doi.org/10.1029/2022EF003474>, 2024.
- 706 Lim, C. H., Ryu, J., Choi, Y., Jeon, S. W., and Lee, W. K.: Understanding global PM<sub>2.5</sub> concentrations and their drivers in recent  
707 decades (1998–2016), *Environ. Int.*, 144, 106011, <https://doi.org/10.1016/j.envint.2020.106011>, 2020.
- 708 Lin, H., Feng, X., Fu, T.-M., Tian, H., Ma, Y., Zhang, L., Jacob, D. J., Yantosca, R. M., Sulprizio, M. P., Lundgren, E. W.,  
709 Zhuang, J., Zhang, Q., Lu, X., Zhang, L., Shen, L., Guo, J., Eastham, S. D., and Keller, C. A.: WRF-GC (v1.0): online  
710 coupling of WRF (v3.9.1.1) and GEOS-Chem (v12.2.1) for regional atmospheric chemistry modeling – Part 1:  
711 Description of the one-way model, *Geosci. Model Dev.*, 13, 3241–3265, <https://doi.org/10.5194/gmd-13-3241-2020>, 2020
- 712 Liu, J., Jin, J., and Niu, G.-Y.: Effects of irrigation on seasonal and annual temperature and precipitation over China simulated  
713 by the WRF model, *J. Geophys. Res.: Atmos.*, 126, e2020JD034222, <https://doi.org/10.1029/2020JD034222>, 2021a.
- 714 Liu, K., Bo, Y., Li, X., Wang, S., and Zhou, G.: Uncovering current and future variations of irrigation water use across China  
715 using machine learning, *Earth's Future*, 12, e2023EF003562, <https://doi.org/10.1029/2023EF003562>, 2024a.
- 716 Liu, G., Wang, W., Shao, Q., Wei, J., Zheng, J., Liu, B., and Chen, Z.: Simulating the climatic effects of irrigation over China  
717 by using the WRF-Noah model system with mosaic approach, *J. Geophys. Res.: Atmos.*, 126, e2020JD034428,  
718 <https://doi.org/10.1029/2020JD034428>, 2021b.
- 719 Liu, X., Chu, B., Tang, R., Liu, Y., Qiu, B., Gao, M., Li, X., Xiao, J., Sun Zhe, H., Huang, X., Desai, A. R., Ding, A., and  
720 Wang, H.: Air quality improvements can strengthen China's food security, *Nat Food*, 5, 158–170.  
721 <https://doi.org/10.1038/s43016-023-00882-y>, 2024b.
- 722 Liu, Z., Zhou, M., Chen, Y., Chen, D., Pan, Y., Song, T., Ji, D., Chen, Q., and Zhang, L.: The nonlinear response of fine  
723 particulate matter pollution to ammonia emission reductions in North China, *Environ. Res. Lett.*, 16(3), 034014,  
724 <https://doi.org/10.1088/1748-9326/abdf86>, 2021c.
- 725 Liu, J., Kuang, W., Zhang, Z., Xu, X., Qin, X., Qin, Y., Ning, J., Zhou, W., Zhang, S., Li, R., Yan, C., Wu, S., Shi, X., Jiang,  
726 N., Yu, D., Pan, X., and Chi, W.: Spatiotemporal characteristics, patterns, and causes of land-use changes in China since  
727 the late 1980s, *J Geog Sci*, 24, 195–210, <https://doi.org/10.1007/s11442-014-1082-6>, 2014.
- 728 Lobell, D. B., Bonfils, C. J., Kueppers, L. M., and Snyder, M. A.: Irrigation cooling effect on temperature and heat index  
729 extremes, *Geophys. Res. Lett.*, 35, L09705, <https://doi.org/10.1029/2008GL034145>, 2008.
- 730 Lu, X., Hong, J., Zhang, L., Cooper, O. R., Schultz, M. G., Xu, X., Wang, T., Gao, M., Zhao, Y. and Zhang, Y.: Severe surface  
731 ozone pollution in China: a global perspective. *Environ. Sci. Technol. Lett.*, 5, 487–494.  
732 <https://doi.org/10.1021/acs.estlett.8b00366>, 2018.
- 733 Lu, X., Zhang, L., and Shen, L.: Meteorology and climate influences on tropospheric ozone: a review of natural sources,  
734 chemistry, and transport patterns, *Curr. Pollut. Rep.*, 5, 238–260, <https://doi.org/10.1007/s40726-019-00118-3>, 2019.
- 735 Mao, J., Tai, A. P. K., Yung, D. H. Y., Yuan, T., Chau, K. T., and Feng, Z.: Multidecadal ozone trends in China and implications  
736 for human health and crop yields: a hybrid approach combining a chemical transport model and machine learning, *Atmos.*  
737 *Chem. Phys.*, 24, 345–366, <https://doi.org/10.5194/acp-24-345-2024>, 2024.
- 738 McDermid, S., Nocco, M., Lawston-Parker, P., Keune, J., Pokhrel, Y., Jain, M., Jägermeyr, J., Brocca, L., Massari, C., Jones,



- 739 A. D., Vahmani, P., Thiery, W., Yao, Y., Bell, A., Chen, L., Dorigo, W., Hanasaki, N., Jasechko, S., Lo, M.-H., Mahmood,  
740 R., Mishra, V., Muller, N. D., Niyogi, D., Rabin, S. S., Sloat, L., Wada, Y., Zappa, L., Chen, F., Cook, B. I., Kim, H.,  
741 Lombardozi, D., Polcher, J., Ryu, D., Santanello, J., Satoh, Y., Seneviratne, S., Singh, D. and Yokohata, T.: Irrigation in  
742 the Earth system, *Nat. Rev. Earth Environ.*, 1–19, <https://doi.org/10.1038/s43017-023-00438-5>, 2023.
- 743 Morrison, H., Thompson, G., and Tatarskii, V.: Impact of Cloud Microphysics on the Development of Trailing Stratiform  
744 Precipitation in a Simulated Squall Line: Comparison of One- and Two-Moment Schemes, *Mon. Weather Rev.*, 137, 991–  
745 1007, <https://doi.org/10.1175/2008MWR2556.1>, 2009.
- 746 Niu, G. Y., Yang, Z. L., Mitchell, K. E., Chen, F., Ek, M. B., Barlage, M., Kumar, A., Manning, K., Niyogi, D., Rosero, E.,  
747 Tewari, M., Xia, Y.: The community Noah land surface model with multiparameterization options (Noah-MP): 1. Model  
748 description and evaluation with local-scale measurements, *J. Geophys. Res.: Atmos.*, 116, D12109,  
749 <https://doi.org/10.1029/2010JD015139>, 2011.
- 750 Nakanishi, M. and Niino, H.: An improved Mellor-Yamada level-3 model: Its numerical stability and application to a regional  
751 prediction of advection fog, *Bound.-Lay. Meteorol.*, 119, 397–407, <https://doi.org/10.1007/s10546-005-9030-8>, 2006.
- 752 Pye, H. O. T., Liao, H., Wu, S., Mickley, L. J., Jacob, D. J., Henze, D. K., and Seinfeld, J. H.: Effect of changes in climate and  
753 emissions on future sulfate-nitrate-ammonium aerosol levels in the United States, *J. Geophys. Res.-Atmos.*, 114, D01205,  
754 <https://doi.org/10.1029/2008JD010701>, 2009.
- 755 Qi, X., Feng, K., Sun, L., Zhao, D., Huang, X., Zhang, D., Liu, Z., and Baiocchi, G.: Rising agricultural water scarcity in China  
756 is driven by expansion of irrigated cropland in water scarce regions, *One Earth*, 5, 1139–1152,  
757 <https://doi.org/10.1016/j.oneear.2022.09.008>, 2022.
- 758 Qian, Y., Yang, Z., Feng, Z., Liu, Y., Gustafson, W. I., Berg, L. K., Huang, M., Yang, B., and Ma, H. Y.: Neglecting irrigation  
759 contributes to the simulated summertime warm-and-dry bias in the central United States, *npj Clim Atmos Sci* 3, 31.  
760 <https://doi.org/10.1038/s41612-020-00135-w>, 2020.
- 761 Qian, J., Liao, H., Yang, Y., Li, K., Chen, L., and Zhu, J.: Meteorological influences on daily variation and trend of summertime  
762 surface ozone over years of 2015–2020: Quantification for cities in the Yangtze River Delta, *Sci. Total Environ.*, 834,  
763 155107, <https://doi.org/10.1016/j.scitotenv.2022.155107>, 2022.
- 764 Randerson, J. T., van der Werf, G. R., Giglio, L., Collatz, G. J., and Kasibhatla, P. S.: Global Fire Emissions Database, Version  
765 4, (GFEDv4). ORNL DAAC, Oak Ridge, Tennessee, USA., <https://doi.org/10.3334/ORNLDAAC/1293>, 2018
- 766 Ren, J., Guo, F., and Xie, S.: Diagnosing ozone–NO<sub>x</sub>–VOC sensitivity and revealing causes of ozone increases in China based  
767 on 2013–2021 satellite retrievals, *Atmos. Chem. Phys.*, 22, 15035–15047, <https://doi.org/10.5194/acp-22-15035-2022>,  
768 2022
- 769 Sacks, W. J., Cook, B. I., Buening, N., Levis, S., and Helkowski, J. H.: Effects of global irrigation on the near-surface climate,  
770 *Clim. Dyn.*, 33(2–3), 159–175, <https://doi.org/10.1007/s00382-008-0445-z>, 2009.
- 771 Shen, Y., Xiao, Z., Wang, Y., Xiao, W., Yao, L., and Zhou, C.: Impacts of agricultural soil NO<sub>x</sub> emissions on O<sub>3</sub> over mainland  
772 China. *J. Geophys. Res.: Atmos.*, 128, e2022JD037986. <https://doi.org/10.1029/2022JD037986>, 2023.
- 773 Shi, Z., Song, C., Liu, B., Lu, G., Xu, J., Van Vu, T., Elliott, R. J. R., Li, W., Bloss, W. J., and Harrison, R. M.: Abrupt but  
774 smaller than expected changes in surface air quality attributable to COVID-19 lockdowns. *Sci. Adv.*, 7(3), eabd6696,  
775 <https://doi.org/10.1126/sciadv.abd6696>, 2021.



- 776 Shi, Z., Huang, L., Li, J., Ying, Q., Zhang, H., and Hu, J.: Sensitivity analysis of the surface ozone and fine particulate matter  
777 to meteorological parameters in China, *Atmos. Chem. Phys.*, 20(21), 13455–13466, [https://doi.org/10.5194/acp-20-](https://doi.org/10.5194/acp-20-13455-2020)  
778 [13455-2020](https://doi.org/10.5194/acp-20-13455-2020), 2020.
- 779 Skamarock, W. C., Klemp, J. B., Dudhia, J., Gill, D. O., Barker, D., Duda, M. G., Hunag, X., Wang, W., and Powers, J. G.:  
780 NCAR Tech. Note NCAR/TN-475+STR: A Description of the Advanced Research WRF Model Version 3,  
781 <https://doi.org/10.5065/D68S4MVH>, 2008
- 782 Sorooshian, S., Li, J., Hsu, K., and Gao, X.: Influence of irrigation schemes used in RCMs on ET estimation: results and  
783 comparative studies from California's Central Valley agricultural regions, *J. Geophys. Res.*, 117, D06107,  
784 <http://dx.doi.org/10.1029/2011JD016978>, 2012.
- 785 Sorooshian, S., AghaKouchak, A., and Li, J.: Influence of irrigation on land hydrological processes over California, *J. Geophys.*  
786 *Res. Atmos.*, 119, 13137–13152, <http://dx.doi.org/10.1002/2014JD022232>, 2014.
- 787 Song, C., Jiao, Y., Yang, W., Yu, Y., Zhang, J., and Liu, Y.: Research progress on the influence of irrigation methods on ammonia  
788 volatilization in farmland, *IOP Conference Series: Earth and Environmental Science*. IOP Publishing, 647(1), 012170,  
789 <http://dx.doi.org/10.1088/1755-1315/647/1/012170>, 2021.
- 790 Sun, J., Liu, L., Xu, L., Wang, Y., Wu, Z., Hu, M., Shi, Z., Li, Y., Zhang, X., Chen, J., Li, W.: Key role of nitrate in phase  
791 transitions of urban particles: Implications of important reactive surfaces for secondary aerosol formation. *J. Geophys.*  
792 *Res. Atmos.*, 123, 1234–1243, <https://doi.org/10.1002/2017JD027264>, 2018.
- 793 Sun, J., Qin, M., Xie, X., Fu, W., Qin, Y., Sheng, L., Li, L., Li, J., Sulaymon, I. D., Jiang, L., Huang, L., Yu, X., and Hu, J.:  
794 Seasonal modeling analysis of nitrate formation pathways in Yangtze River Delta region, China, *Atmos. Chem. Phys.*, 22,  
795 12629–12646, <https://doi.org/10.5194/acp-22-12629-2022>, 2022.
- 796 Tai, A. P., Mickley, L. J., and Jacob, D. J.: Correlations between fine particulate matter (PM<sub>2.5</sub>) and meteorological variables  
797 in the United States: Implications for the sensitivity of PM<sub>2.5</sub> to climate change, *Atmos. Environ.*, 44(32), 3976–3984,  
798 <https://doi.org/10.1016/j.atmosenv.2010.06.060>, 2010.
- 799 Tai, A. P. K., Mickley, L. J., Jacob, D. J., Leibensperger, E. M., Zhang, L., Fisher, J. A., and Pye, H. O. T.: Meteorological  
800 modes of variability for fine particulate matter (PM<sub>2.5</sub>) air quality in the United States: implications for PM<sub>2.5</sub> sensitivity  
801 to climate change, *Atmos. Chem. Phys.*, 12, 3131–3145, <https://doi.org/10.5194/acp-12-3131-2012>, 2012.
- 802 Tai, A. P., Martin, M. V., and Heald, C. L.: Threat to future global food security from climate change and ozone air pollution,  
803 *Nat. Clim. Change*, 4(9), 817–821, <https://doi.org/10.1038/NCLIMATE2317>, 2014.
- 804 Tie, X., Huang, R. J., Cao, J., Zhang, Q., Cheng, Y., Su, H., Chang, D., Pöschl, U., Hoffmann, T., Dusek, U., Li, G., Worsnop,  
805 D. R., and O'Dowd, C. D.: Severe Pollution in China Amplified by Atmospheric Moisture, *Sci. Rep.* 7, 15760,  
806 <https://doi.org/10.1038/s41598-017-15909-1>, 2017.
- 807 Tiedtke, M.: A comprehensive mass flux scheme for cumulus parameterization in large-scale models, *Mon. Weather. Rev.*, 117,  
808 1779–1800, [https://doi.org/10.1175/1520-0493\(1989\)117<1779:ACMFSF>2.0.CO;2](https://doi.org/10.1175/1520-0493(1989)117<1779:ACMFSF>2.0.CO;2), 1989.
- 809 Travis, K. R., Crawford, J. H., Chen, G., Jordan, C. E., Nault, B. A., Kim, H., Jimenez, J. L., Campuzano-Jost, P., Dibb, J. E.,  
810 Woo, J.-H., Kim, Y., Zhai, S., Wang, X., McDuffie, E. E., Luo, G., Yu, F., Kim, S., Simpson, I. J., Blake, D. R., Chang,  
811 L., and Kim, M. J.: Limitations in representation of physical processes prevent successful simulation of PM<sub>2.5</sub> during  
812 KORUS-AQ, *Atmos. Chem. Phys.*, 22, 7933–7958, <https://doi.org/10.5194/acp-22-7933-2022>, 2022.



- 813 Wang, L., Zhao, B., Zhang, Y., and Hu, H.: Correlation between surface PM<sub>2.5</sub> and O<sub>3</sub> in eastern China during 2015–2019:  
814 Spatiotemporal variations and meteorological impacts, *Atmos. Environ.*, 294, 119520,  
815 <https://doi.org/10.1016/j.atmosenv.2022.119520>, 2023.
- 816 Wang, W., Parrish, D. D., Wang, S., Bao, F., Ni, R., Li, X., Yang, S., Wang, H., Cheng, Y., and Su, H.: Long-term trend of  
817 ozone pollution in China during 2014–2020: distinct seasonal and spatial characteristics and ozone sensitivity, *Atmos.*  
818 *Chem. Phys.*, 22, 8935–8949, <https://doi.org/10.5194/acp-22-8935-2022>, 2022a.
- 819 Wang, T., Xue, L., Feng, Z., Dai, J., Zhang, Y., and Tan, Y.: Ground-level ozone pollution in China: a synthesis of recent  
820 findings on influencing factors and impacts, *Environ. Res. Lett.*, 17(6), 063003. <https://doi.org/10.1088/1748-9326/ac69fe>,  
821 [2022b](https://doi.org/10.1088/1748-9326/ac69fe).
- 822 Wang, H., Huang, C., Tao, W., Gao, Y., Wang, S., Jing, S., Wang, W., Yan, R., Wang, Q., An, J., Tian, J., Hu, Q., Lou, S., Pöschl,  
823 U., Cheng, y., Su, H.: Seasonality and reduced nitric oxide titration dominated ozone increase during COVID-19  
824 lockdown in eastern China, *npj Clim. Atmos. Sci.*, 5, 24, <https://doi.org/10.1038/s41612-022-00249-3>, 2022c.
- 825 Wang, T., Xue, L., Brimblecombe, P., Lam, Y. F., Li, L., and Zhang, L.: Ozone pollution in China: A review of concentrations,  
826 meteorological influences, chemical precursors, and effects, *Sci. Total Environ.*, 575, 1582–1596,  
827 <https://doi.org/10.1016/j.scitotenv.2016.10.081>, 2017.
- 828 Wang, Y., Gao, W., Wang, S., Song, T., Gong, Z., Ji, D., Wang, L., Liu, Z., Tang, G., Huo, Y., Tian, S., Li, J., Li, M., Yang, Y.,  
829 Chu, B., Petäjä, T., Kerminen, V.-M., He, H., Hao, J., Kulmala, M., Wang, Y., and Zhang, Y.: Contrasting trends of PM<sub>2.5</sub>  
830 and surface-ozone concentrations in China from 2013 to 2017, *Natl. Sci. Rev.*, 7(8), 1331–1339,  
831 <https://doi.org/10.1093/nsr/nwaa032>, 2020.
- 832 Xu, T., Zhang, C., Liu, C., and Hu, Q.: Variability of PM<sub>2.5</sub> and O<sub>3</sub> concentrations and their driving forces over Chinese  
833 megacities during 2018–2020, *J. Environ. Sci.*, 124, 1–10, <https://doi.org/10.1016/j.jes.2021.10.014>, 2023.
- 834 Xue, L. K., Wang, T., Gao, J., Ding, A. J., Zhou, X. H., Blake, D. R., Wang, X. F., Saunders, S. M., Fan, S. J., Zuo, H. C.,  
835 Zhang, Q. Z., and Wang, W. X.: Ground-level ozone in four Chinese cities: precursors, regional transport and  
836 heterogeneous processes, *Atmos. Chem. Phys.*, 14, 13175–13188, <https://doi.org/10.5194/acp-14-13175-2014>, 2014.
- 837 Yang, B., Zhang, Y., Qian, Y., Tang, J., and Liu, D.: Climatic effects of irrigation over the Huang-Huai-Hai Plain in China  
838 simulated by the weather research and forecasting model, *J. Geophys. Res.: Atmos.*, 5(121), 2246–2264,  
839 <https://doi.org/10.1002/2015JD023736>, 2015.
- 840 [Yang, Y., Jin, Z., Mueller, N. D., Driscoll, A. W., Hernandez, R. R., Grodsky, S. M., Sloat, L. L., Chester, M. V., Zhu, Y.-G.,  
841 and Lobell, D. B.: Sustainable irrigation and climate feedbacks, \*Nat. Food\*, 1–10, \[https://doi.org/10.1038/s43016-023-  
842 00821-x\]\(https://doi.org/10.1038/s43016-023-00821-x\), 2023.](https://doi.org/10.1038/s43016-023-00821-x)
- 843 [Yang, J., and Zhao, Y.: Performance and application of air quality models on ozone simulation in China – A review, \*Atmos.\*  
844 \*Environ.\*, 293, 119446, <https://doi.org/10.1016/j.atmosenv.2022.119446>, 2023.](https://doi.org/10.1016/j.atmosenv.2022.119446)
- 845 [Ye, X., Wang, X., and Zhang, L.: Diagnosing the model bias in simulating daily surface ozone variability using a machine  
846 learning method: The effects of dry deposition and cloud optical depth, \*Environ. Sci. Technol.\*, 56, 16665–16675,  
847 <https://doi.org/10.1021/acs.est.2c05712>, 2022.](https://doi.org/10.1021/acs.est.2c05712)
- 848 Yin, H., Liu, C., Hu, Q.H., Liu, T., Wang, S.T., Gao, M., Xu, S.Q., Zhang, C.X., Su, W.J.: Opposite impact of emission reduction  
849 during the COVID-19 lockdown period on the surface concentrations of PM<sub>2.5</sub> and O<sub>3</sub> in Wuhan, China., *Environ. Pollut.*,



- 850 289, 11. <https://doi.org/10.1016/j.envpol.2021.117899>, 2021.
- 851 Yuan, T., Tai, A. P. K., Mao, J., Tam, O., H. F., Li, R. K. K., Wu, J., and Li, S.: Effects of different irrigation methods on regional  
852 climate in North China Plain: A modeling study, *Agric. For. Meteorol.*, 342, 109728,  
853 <https://doi.org/10.1016/j.agrformet.2023.109728>, 2023.
- 854 Zender, C. S., Bian, H., and Newman, D.: Mineral Dust Entrainment and Deposition (DEAD) model: Description and 1990s  
855 dust climatology, *J. Geophys. Res.-Atmos.*, 108, 4416, <https://doi.org/10.1029/2002JD002775>, 2003
- 856 Zhai, S., Jacob, D. J., Wang, X., Liu, Z., Wen, T., Shah, V., Li, K., Moch, J. M., Bates, K. H., Song, S., Shen, L., Zhang, Y.,  
857 Luo, G., Yu, F., Sun, Y., Wang, L., Qi, M., Tao, J., Gui, K., Xu, H., Zhang, Q., Zhao, T., Wang, Y., Lee, H. C., Choi, H.,  
858 and Liao, H.: Control of particulate nitrate air pollution in China, *Nat. Geosci.*, 14(6), 389–395,  
859 <https://doi.org/10.1038/s41561-021-00726-z>, 2021.
- 860 Zhang, C., Dong, J. and Ge, Q.: Mapping 20 years of irrigated croplands in China using MODIS and statistics and existing  
861 irrigation products, *Sci. Data*, 9, 407. <https://doi.org/10.1038/s41597-022-01522-z>, 2022.
- 862 Zhang, C., Wang, Y., and Hamilton, K.: Improved representation of boundary layer clouds over the southeast Pacific in ARW-  
863 WRF using a modified Tiedtke cumulus parameterization scheme, *Mon. Weather Rev.*, 139, 3489–3513,  
864 <https://doi.org/10.1175/MWR-D-10-05091.1>, 2011
- 865 Zhang, Y. L. and Cao, F.: Fine particulate matter (PM<sub>2.5</sub>) in China at a city level, *Sci. Rep.*, 5(1), 1–12,  
866 <https://doi.org/10.1038/srep14884>, 2015.
- 867 Zhao, H., Chen, K., Liu, Z., Zhang, Y., Shao, T., and Zhang, H.: Coordinated control of PM<sub>2.5</sub> and O<sub>3</sub> is urgently needed in  
868 China after implementation of the “Air pollution prevention and control action plan”, *Chemosphere*, 270, 129441,  
869 <https://doi.org/10.1016/j.chemosphere.2020.129441>, 2021.
- 870 Zheng, B., Tong, D., Li, M., Liu, F., Hong, C., Geng, G., Li, H., Li, X., Peng, L., Qi, J., Yan, L., Zhang, Y., Zhao, H., Zheng,  
871 Y., He, K., and Zhang, Q.: Trends in China’s anthropogenic emissions since 2010 as the consequence of clean air actions,  
872 *Atmos. Chem. Phys.*, 18, 14095–14111, doi: 10.5194/acp-18-14095-2018, 2018.
- 873 Zhou, F., Bo, Y., Ciais, P., Dumas, P., Tang, Q., Wang, X., Liu, J., Zheng, C., Polcher, J., Yin, Z., Guimberteau, M., Peng, S.,  
874 Otle, C., Zhao, X., Zhao, J., Tan, Q., Chen, L., Shen, H., Yang, H., Piao, S., Wang, H., and Wada, Y.: Deceleration of  
875 China’s human water use and its key drivers, *Proc. Natl. Acad. Sci. U.S.A.*, 117(14), 7702–7711,  
876 <https://doi.org/10.1073/pnas.1909902117>, 2020.
- 877 [Zhang, L., Zheng, D., Zhang, K., Chen, H., Ge, Y., and Li, X.: Divergent trends in irrigation-water withdrawal and consumption  
878 over mainland China, \*Environ. Res. Lett.\*, 17, 094001, <https://doi.org/10.1088/1748-9326/ac8606>, 2022.](https://doi.org/10.1016/j.envres.2022.1094001)
- 879 Zhou, S. S., Tai, A. P. K., Sun, S., Sadiq, M., Heald, C. L., and Geddes, J. A.: Coupling between surface ozone and leaf area  
880 index in a chemical transport model: strength of feedback and implications for ozone air quality and vegetation health,  
881 *Atmos. Chem. Phys.*, 18, 14133–14148, <https://doi.org/10.5194/acp-18-14133-2018>, 2018.
- 882 Zhu, J., Tai, A. P. K., and Hung Lam Yim, S.: Effects of ozone–vegetation interactions on meteorology and air quality in China  
883 using a two-way coupled land–atmosphere model, *Atmos. Chem. Phys.*, 22, 765–782, [https://doi.org/10.5194/acp-22-  
884 765-2022](https://doi.org/10.5194/acp-22-765-2022), 2022.
- 885